A Unified Tensor-Based Joint AUD and ISAC Parameter Estimation With Large-Scale User Access

Tiancheng Yang, Dongxuan He, *Member, IEEE*, Huazhou Hou, *Member, IEEE*, Hua Wang, *Member, IEEE*, Hao Yin, Yongming Huang, *Fellow, IEEE*, Zhaocheng Wang, *Fellow, IEEE*, and Tony Q. S. Quek, *Fellow, IEEE*

Abstract—The integration of active user detection (AUD) and integrated sensing and communication (ISAC) enables the realization of communication and sensing functionalities over one hardware platform within the realm of ultra-massive machine-type communications (umMTC). However, the coupling of communication and sensing signals at the receiver poses challenges in accurately acquiring the respective parameters for both functionalities. In this paper, a unified tensor-based joint communication and sensing parameter estimation algorithm is proposed. First, leveraging CANDECOMP/PARAFAC decomposition (CPD), the channel model is converted into a unified tensor-based form, facilitating effective processing of the received signals. Subsequently, a two-stage CPD-based unified communication and sensing parameter estimation algorithm is developed. In the first stage, the factor matrix is estimated by utilizing the matrix subspace-based method and the Vandermonde property of the matrix. In the second stage, equivalent path parameters are extracted based on the estimated factor matrices. Furthermore, to solve the coupling problem of equivalent path parameters, a joint alternating iterative pilot-channel estimation (JAI-PCE) algorithm is proposed, effectively decoupling and accurately estimating the parameters. Simulation results verify the effectiveness of our proposed algorithm in terms of AUD, channel estimation, and radar sensing.

Tiancheng Yang, Dongxuan He, and Hua Wang are with the School of Information and Electronics, Beijing Institute of Technology, Beijing 100081, China (e-mail: tiancheng_yang@bit.edu.cn; dongxuan_he@bit.edu.cn; wanghua@bit.edu.cn).

Huazhou Hou is with the Pervasive Communication Research Center, Purple Mountain Laboratories, Nanjing 211111, China (e-mail: houhuazhou@pmlabs.com.cn).

Hao Yin is with the Institute of Systems Engineering, Academy of Military Sciences, Beijing, 100141, China (e-mail: yinhao@cashq.ac.cn).

Yongming Huang is with the School of Information Science and Engineering, Southeast University, Nanjing 210096, China, and also with the Pervasive Communication Research Center, Purple Mountain Laboratories, Nanjing 211111, China (e-mail: huangym@seu.edu.cn).

Zhaocheng Wang is with the Beijing National Research Center for Information Science and Technology, Department of Electronic Engineering, Tsinghua University, Beijing 100084, China (e-mail: zcwang@tsinghua.edu.cn).

Tony Q. S. Quek is with the Information Systems Technology and Design, Singapore University of Technology and Design, Singapore 487372 (e-mail: tonyquek@sutd.edu.sg).

Digital Object Identifier 10.1109/TCCN.2025.3545690

Index Terms—Active user detection, integrated sensing and communication, CANDECOMP/PARAFAC decomposition, tensor decomposition, joint communication and sensing parameter estimation.

I. Introduction

ULTRA-MASSIVE machine-type communications (umMTC) is a key application scenario in the sixth generation (6G) networks to support the connection of an enormous number of devices [1], which plays a critical role in various fields including intelligent transportation, autonomous industries, smart cities, etc [2]. In these domains, the number of connected devices has increased significantly, resulting in an urgent demand for massive device connection and efficient data processing. However, the surge in connected devices has brought new challenges. On the one hand, the requirement of massive device connection has made base stations (BSs) resource scheduling difficult, where BSs must identify active devices to provide high-quality communication services with the help of grant-free random access (GF-RA) [3]. On the other hand, sensing function is required to achieve location positioning and environmental monitoring, thus making integrated sensing and communication (ISAC) become an indispensable key technology [4], [5].

More specifically, active user detection (AUD) can ensure access performance for large-scale users and reduce complexity of BS resource scheduling in GF-RA scenarios, which has been proven to be a potential technology for umMTC scenarios [6]. Besides, ISAC, which aims to achieve both communication and sensing functionalities in the same frequency and equipment, is emerging as a promising technology in future 6G networks [7]. For both AUD and ISAC, accurate parameter estimation poses tricky challenges. The received signals are typically coupled in both AUD and ISAC, resulting in high-dimensional mixed data that complicates the estimation of communication and sensing parameters [8], [9].

Recently, some works have been proposed to perform the parameter estimation in AUD and ISAC [9], [10], [11], [12], [13], [14], [15]. For AUD, focusing only on solving the AUD problem, the advanced algorithms based on the orthogonal matching pursuit (OMP) have been proposed [10], [11]. In [10], the multi-user signals can be detected simultaneously in multiple consecutive time slots, while OMP is used to handle each time slot independently. In [11], two innovative algorithms were proposed to solve the AUD problem even under inaccurate pilot estimation, without requiring the

TABLE I
A COMPARISON OF THE RELATED LITERATURE WITH OUR WORK

Reference	Scenario	Transmission mode	Communication Users	Sensing Targets
[8]	Communication	Downlink	Single	/
[17]	Communication	Downlink	Single	/
[18]	Communication + Sensing	Downlink	Single	Multiple
[19]	Communication	Uplink	Multiple	/
Our work	Communication + Sensing	Uplink + Downlink	Large-scale	Multiple

sparsity level of user activity. In addition, joint channel state information (CSI) estimation and AUD methods were proposed in [9] and [12]. In [9], the approximate message passing (AMP) algorithm was introduced in compressed sensing to improve the accuracy of CSI estimation and the performance of AUD simultaneously, while the complexity of the above method is typically too high. In [12], the performance of AUD and channel estimation based on the AMP algorithm with non-orthogonal pilot sequences was derived theoretically, providing theoretical support for the trade-offs between channel estimation accuracy and effective data throughput in massive connectivity scenarios. For ISAC, accurate estimation of communication and sensing parameters typically requires partially known communication channel states or target parameter information [13], [14], [15]. For example, the authors in [13] proposed a transformer-based sliding symbol detection algorithm that necessitates a channel matrix estimated by the least-squares (LS) algorithm for communication data detection and target parameter estimation. A delay-Doppler-angle estimation algorithm was proposed to estimate the parameters for multiple-input multiple-output (MIMO)-ISAC systems in [14], which needs the accurate communication CSI to efficiently estimate the target parameters. In [15], a bilinear unitary approximate message passing algorithm is proposed to jointly perform channel estimation and signal detection, requiring accurate sensing parameters as prior information.

The tensor theory, which excels in handling high-dimensional data, was introduced in signal processing [8], [16], [17], [18], [19], [20]. The authors in [16] developed a tensor generalized block OMP algorithm to address the problem of sparse tensor recovery from its compressed representation, by introducing a holistic mutual incoherence property of the measurement matrix set. In [17], a CANDECOMP/PARAFAC decomposition (CPD)-based method for channel parameter estimation was first introduced in millimeter-wave (mmWave) MIMO-orthogonal frequency-division multiplexing (OFDM) systems. However, the considered channel model ignores the effect of Doppler shift, thus limiting the system performance in practical scenarios. To tackle this issue, the authors in [8] proposed a tensor decomposition-based method to realize the channel estimation in high mobility scenarios with severe Doppler effect. The authors in [18] proposed a joint tensor-based algorithm to estimate the communication and sensing parameters simultaneously in ISAC, which shows outstanding performance in estimation accuracy, sensing resolution, and

training pilot overhead. However, the scenario considering large-scale users has not been studied. In [19], a CPD-based algorithm was proposed to estimate the communication parameters according to the time domain channel matrix in an uplink system with one BS and multiple user equipments (UEs), capable of saving pilot overhead without significant performance loss. However, obtaining communication and sensing parameters in the context of large-scale user access combined with ISAC remains challenging due to the intricate coupling of received signals, which motivates us to explore new algorithms to address this issue. For clarity, Table I is presented to compare our work with the related tensor-based works.

In this paper, a unified tensor-based joint communication and sensing parameter estimation algorithm is proposed to estimate the communication and sensing parameters for ISAC with large-scale user access. The main contributions of the paper are summarized as follows:

1) The scenario of joint AUD and ISAC is first proposed, allowing a large number of uplink users to communicate with an ISAC BS, which can simultaneously detect multiple targets. For instance, this could be applied in smart cities, autonomous industries, intelligent transportation, etc. Specifically, our considered joint AUD and ISAC can support numerous devices for communication and sensing. Compared to small-scale user access scenarios, the joint AUD and ISAC scenario faces significant challenge in terms of computational complexity. The increased number of users and targets results in a greater coupling of received signals, thus making the estimation of communication and sensing parameters much more difficult. Furthermore, the equivalent channel and signal models corresponding to this scenario are derived.

2) A unified tensor-based channel model for communication and sensing parameter estimation is proposed. In particular, both communication and radar parameters are converted into equivalent path parameters, which enables effective estimation of the coupled communication and radar parameters.

3) A matrix subspace-based method relying on Vandermonde structure is proposed to accurately estimate the factor matrix in scenarios involving joint AUD and ISAC. A joint alternating iterative pilot-channel estimation (JAI-PCE) algorithm is further developed to solve the coupling problem of equivalent
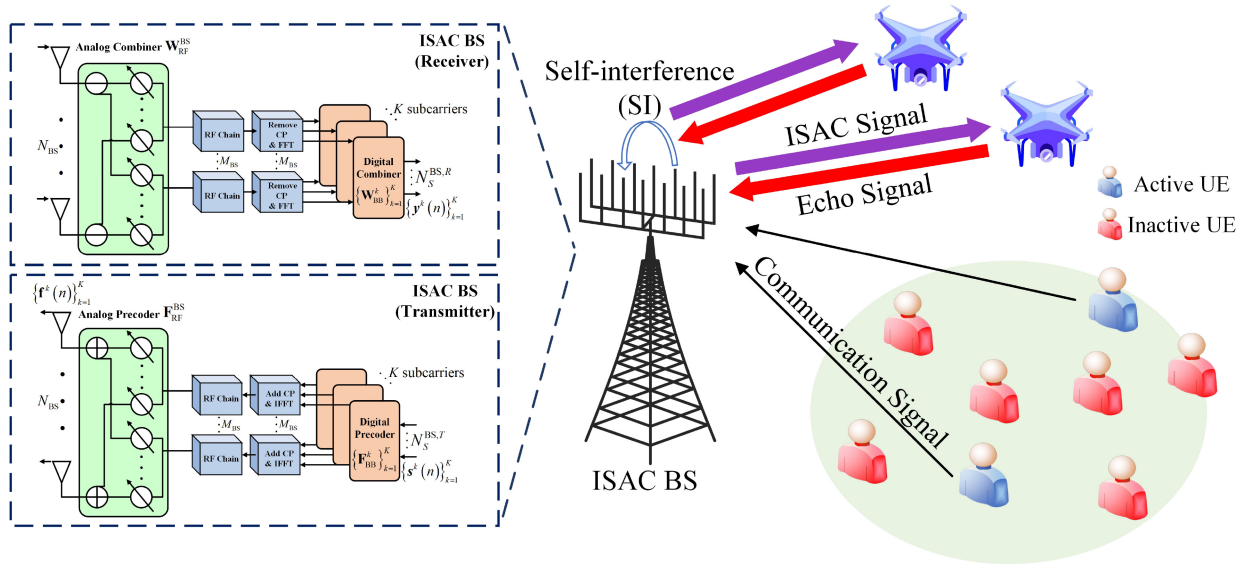
Fig. 1. An illustration of the considered ISAC system, where an ISAC BS with hybrid beamforming architectures simultaneously serves multiple communication users and performs target sensing.

path parameters. Leveraging pilot estimation, the estimated path parameters can be uniquely associated with the communication UEs, effectively resolving the identification issue caused by permutation matrices in the CPD-based unified parameter estimation algorithm.

The rest of this paper is organized as follows. In Section II, we study the communication and radar channels and signal models for the scenario of joint AUD and ISAC. Section III proposes a unified tensor-based channel for communication and sensing, and then analyzes the uniqueness condition of the CPD problem. In Section IV, we propose a two-stage CPD-based unified communication channel and sensing targets parameter estimation algorithm and perform the complexity analysis. Besides, a JAI-PCE algorithm is also proposed in this section. Simulation results are presented in Section V, followed by conclusions in Section VI.

Notations: Scalars, vectors, matrices, and tensors are denoted by lowercase letters, lowercase boldface letters, uppercase boldface letters, and Euler script letters, respectively. The transpose, conjugate transpose, conjugate, inverse and Moore-Penrose pseudo-inverse operations are represented by $(\cdot)^T$, $(\cdot)^H$, $(\cdot)^*$, $(\cdot)^{-1}$ and $(\cdot)^\dagger$, respectively. The outer product, Kronecker product, and Khatri-Rao product are denoted by $\circ$, $\otimes$, and $\odot$, respectively. $\|\cdot\|_F$ and $\|\cdot\|_2$ are the Frobenius norm and l_2 norm, respectively. $\text{Re}\{A\}$ is the real part of the complex number A, while $\mathbf{I}_N$ is the $N \times N$ identity matrix. $[\![\cdot]\!]$ is the Kruskal operator, and $\mathcal{CN}(0, \sigma^2)$ is the circularly-symmetric complex Gaussian distribution with the variance of σ^2. $diag(\mathbf{a})$ returns the diagonal matrix formed by $\mathbf{a}$. $[\mathbf{A}]_{1:m}$ and $[\mathbf{A}]_{:,m}$ are the first m rows of $\mathbf{A}$ and the m-th column of $\mathbf{A}$, respectively. $\cap$ and $[\mathbf{A}]_c$ are the intersection and the total number of elements in set $\mathbf{A}$, respectively.

II. SYSTEM MODEL

As shown in Fig. 1, a mmWave massive MIMO ISAC system is considered in this paper [21], [22], where a full-duplex (FD) ISAC BS equipped with two antenna arrays receives the communication signals from multiple active multiple-antennas uplink UEs and uses the downlink ISAC signals to detect the point radar targets. Particularly, a hybrid beamforming massive MIMO architecture is utilized in this system [23]. It is assumed that N_{BS}^T antennas with M_{BS}^T radio frequency (RF) chains and N_{BS}^R antennas with M_{BS}^R RF chains are employed in the BS for transmission and reception, respectively. Without loss of generality, we assume that $N_{\text{BS}}^T = N_{\text{BS}}^R = N_{\text{BS}}$, $M_{\text{BS}}^T = M_{\text{BS}}^R = M_{\text{BS}}$, and $M_{\text{BS}} < N_{\text{BS}}$. For the uplink communication link, U UEs equipped with N_{UE} antennas and $M_{\text{UE}} = 1$ RF chain send information to the BS, where only λU UEs are active while the remaining $(1 - \lambda)U$ UEs are inactive. More specifically, we assume that $M_{\text{UE}} < N_{\text{UE}}$ and $\lambda \ll 1$. In addition, OFDM signal is used to carry information, where K orthogonal subcarriers are employed to process $N_S^{\text{BS},T}$, $N_S^{\text{BS},R}$, and N_S^{UE} independent data streams, corresponding to the ISAC BS transmitter, ISAC BS receiver, and UE transmitter, respectively. Specifically, subcarriers $\{1, 2, \ldots, \overline{K}\}$ are selected as training subcarriers for parameter estimation. For the downlink ISAC link, the BS sends the OFDM-based ISAC signal to detect Q surrounding targets. The superscript k, subscript u, and subscript q represent the indices of the subcarriers, uplink UEs, and surrounding targets, respectively.

A. Channel Model

For the uplink communication link, suppose a continuous-time baseband communication signal $\tilde{\boldsymbol{s}}_c(t)$ is sent from the n_{UE}-th UE antenna and received at the n_{BS}-th BS antenna via $\tilde{L}_c$ multipaths, and thus the corresponding received continuous-time baseband signal $\tilde{\boldsymbol{y}}_c^{\text{BS}}(t)$ can be obtained, given by [24]

$$\tilde{\boldsymbol{y}}_c^{\text{BS}}(t) = \sum_{l=1}^{\tilde{L}_c} \tilde{\alpha}_l e^{j2\pi\nu_l t} e^{-j2\pi(f_c^{\text{UE}}+\nu_l)\tilde{\tau}_l} \tilde{\boldsymbol{s}}_c(t - \tilde{\tau}_l), \quad (1)$$

where $\tilde{\alpha}_l \in \mathbb{C}$ is the l-th path gain, $\tilde{\alpha}_l = 0$ represents an inactive user, and $\tilde{\alpha}_l \neq 0$ represents an active user. $\nu_l \in \mathbb{R}$ is the Doppler shift of the l-th path that can be expressed by $\nu_l = \frac{v_l}{\lambda_c^{\mathrm{UE}}}$. v_l and λ_c^{UE} are the relative radial velocity of the corresponding uplink UE and the UE's wavelength of the carrier frequency f_c^{UE}, respectively [25]. $\tilde{\tau}_l \geq 0$, which is the time delay from the n_{UE}-th UE antenna to the n_{BS}-th BS antenna, can be presented as

$$\tilde{\tau}_l = \frac{d(n_{\mathrm{UE}} - 1)\sin\phi_l}{c} + \frac{d(n_{\mathrm{BS}} - 1)\sin\theta_l}{c} + \tau_l, \quad (2)$$

where d and c are the adjacent antenna spacing[1] and the light speed, respectively. ϕ_l and θ_l represent the physical real-valued angle of departure (AoD) and angle of arrival (AoA) of the l-th path, respectively, and τ_l denotes the free-space propagation delay from the first UE antenna to the first BS antenna. According to (1) and (2), the corresponding time-domain communication channel matrix $\tilde{\mathbf{H}}(\tau, t)$ can be obtained, given by

$$\tilde{\mathbf{H}}(\tau, t) = \sum_{l=1}^{\tilde{L}_c} \tilde{\alpha}_l e^{j2\pi\nu_l t} e^{-j2\pi(f_c^{\mathrm{UE}} + \nu_l)\tilde{\tau}_l} \delta(\tau - \tilde{\tau}_l)$$
$$= \sum_{l=1}^{\tilde{L}_c} \alpha_l e^{j2\pi\nu_l t} e^{-j2\pi(f_c^{\mathrm{UE}} + \nu_l)(\tau_l^{\mathrm{UE}} + \tau_l^{\mathrm{BS}})} \delta(\tau - \tilde{\tau}_l), \quad (3)$$

where $\alpha_l = \tilde{\alpha}_l e^{-j2\pi(f_c^{\mathrm{UE}} + \nu_l)\tau_l} \in \mathbb{C}$ is the equivalent gain of the l-th path, and $\delta(\cdot)$ is the Dirac delta function. τ_l^{UE} and τ_l^{BS} are equal to $\frac{d(n_{\mathrm{UE}}-1)\sin\phi_l}{c}$ and $\frac{d(n_{\mathrm{BS}}-1)\sin\theta_l}{c}$, respectively. Subsequently, the frequency-domain communication channel matrix $\tilde{\mathbf{H}}(f, t)$ can be obtained by utilizing the Fourier transform on the variable τ of (3), given by

$$\tilde{\mathbf{H}}(f, t) = \sum_{l=1}^{\tilde{L}_c} \alpha_l e^{j2\pi\nu_l t} e^{-j2\pi\left(f_c^{\mathrm{UE}} + \nu_l\right)\left(\tau_l^{\mathrm{UE}} + \tau_l^{\mathrm{BS}}\right)} e^{-j2\pi f\tilde{\tau}_l}$$
$$= \sum_{l=1}^{\tilde{L}_c} \alpha_l e^{j2\pi\nu_l t} e^{-j2\pi\left(f + f_c^{\mathrm{UE}} + \nu_l\right)\left(\tau_l^{\mathrm{UE}} + \tau_l^{\mathrm{BS}}\right)} e^{-j2\pi f\tau_l}$$
$$= \sum_{l=1}^{\tilde{L}_c} \alpha_l e^{-j2\pi\left(f + f_c^{\mathrm{UE}}\right)\tau_l^{\mathrm{UE}}} e^{-j2\pi\left(f + f_c^{\mathrm{UE}}\right)\tau_l^{\mathrm{BS}}} e^{-j2\pi f\tau_l}$$
$$\times e^{j2\pi\nu_l t}, \quad (4)$$

where the Doppler shift ν_l of the l-th path is typically much less than the carrier frequency f_c^{UE}, i.e., $\nu_l \ll f_c^{\mathrm{UE}}$, and thus ν_l can be ignored at the last equality. Ignoring the beam squint effects on antennas and combining the paths of the u-th user antennas sending to the BS antennas, the u-th user's frequency-domain communication channel matrix $\mathbf{H}_u(f, t)$ can be represented as

$$\mathbf{H}_u(f, t) = \sum_{l=1}^{\tilde{L}_c^u} \alpha_l e^{-j2\pi f\tau_l} \mathbf{a}_{\mathrm{BS}}(\theta_l) \mathbf{a}_{\mathrm{UE}}^T(\phi_l) e^{j2\pi\nu_l t}, \quad (5)$$

[1]It is assumed that the adjacent antenna spacing is the same for both the UEs and BS.

where $\tilde{L}_c^u$ denotes the whole number of the multipaths for the u-th user, $\mathbf{a}_{\mathrm{BS}}(\theta_l)$ and $\mathbf{a}_{\mathrm{UE}}(\phi_l)$ are the BS received array steering vector and UEs transmitted array steering vector, respectively, which are given by

$$\mathbf{a}_{\mathrm{BS}}(\theta_l) = \left[1, e^{-j2\pi\frac{d}{\lambda_c^{\mathrm{BS}}}\sin\theta_l}, \ldots, e^{-j2\pi\frac{d(N_{\mathrm{BS}}-1)}{\lambda_c^{\mathrm{BS}}}\sin\theta_l}\right]^T, \quad (6)$$

and

$$\mathbf{a}_{\mathrm{UE}}(\phi_l) = \left[1, e^{-j2\pi\frac{d}{\lambda_c^{\mathrm{UE}}}\sin\phi_l}, \ldots, e^{-j2\pi\frac{d(N_{\mathrm{UE}}-1)}{\lambda_c^{\mathrm{UE}}}\sin\phi_l}\right]^T, \quad (7)$$

respectively. $\lambda_c^{\mathrm{BS}} = \frac{c}{f_c^{\mathrm{BS}}}$ and $\lambda_c^{\mathrm{UE}} = \frac{c}{f_c^{\mathrm{UE}}}$ represent the BS's and UEs' carrier wavelengths, respectively. Subsequently, the communication channel $\mathbf{H}_u^k(n)$ can be obtained by transforming the continuous-time signal into a discrete representation through time and frequency sampling. The considered time-domain and frequency-domain scope are $t \in [nN_{all}T_s, (n+1)N_{all}T_s]$ and $f \in [-f_s/2, f_s/2]$, respectively. $N_{all}T_s = (K + N_{CP})T_s$ is one OFDM symbol time duration, where N_{CP} is the cyclic prefix number in one OFDM symbol, and $f_s = \frac{1}{T_s}$ is the sampling frequency. For the time-domain sampling, the phase duration caused by Doppler shift remains constant within an OFDM symbol [26], and thus $e^{j2\pi\nu_l t} \approx e^{j2\pi\nu_l nN_{all}T_s}$. For the frequency-domain sampling, let $f_s = \frac{kf_s}{K}$, $\mathbf{H}_u^k(n)$ can be denoted as

$$\mathbf{H}_u^k(n) = \mathbf{H}_u\left(\frac{kf_s}{K}, n(K + N_{CP})T_s\right)$$
$$= \sum_{l=1}^{\tilde{L}_c^u} \alpha_l e^{-j2\pi\tau_l f_s\frac{k}{K}} \mathbf{a}_{\mathrm{BS}}(\theta_l) \mathbf{a}_{\mathrm{UE}}^T(\phi_l) e^{j2\pi\nu_l n(K+N_{CP})T_s}, \quad (8)$$

where $1 \leq k \leq \overline{K}$ and $1 \leq n \leq N$.

For the downlink ISAC link, suppose a continuous-time baseband ISAC signal $\tilde{\mathbf{s}}_{ISAC}(t)$ is sent from the n_{BS}^T-th BS antenna and received at the n_{BS}^R-th BS antenna via one path caused by the q-th target, and thus the corresponding received continuous-time baseband echo signal $\tilde{\mathbf{y}}_e^{\mathrm{BS}}(t)$ can be given by [27]

$$\tilde{\mathbf{y}}_e^{\mathrm{BS}}(t) = \tilde{\beta}_q e^{-j2\pi f_c^{\mathrm{BS}}\tilde{\tau}_q} \tilde{\mathbf{s}}_{ISAC}(t - \tilde{\tau}_q), \quad (9)$$

where $\tilde{\beta}_q$ is the q-th target's reflection coefficient caused by two-way transmission path loss and target scattering, and f_c^{BS} is the carrier frequency of the BS. $\tilde{\tau}_q \geq 0$, which is the time delay from the n_{BS}^T-th BS antenna to the n_{BS}^R-th BS antenna, can be given by

$$\tilde{\tau}_q = \frac{d\left(n_{\mathrm{BS}}^T - 1\right)\sin\phi_q}{c} + \frac{d\left(n_{\mathrm{BS}}^R - 1\right)\sin\theta_q}{c} + \frac{2(D_q - v_q t)}{c}, \quad (10)$$

where ϕ_q and θ_q denote the AoD and AoA of the q-th target, respectively. D_q is the distance between the BS and the q-th target, and v_q is the relative radial velocity of the q-th target.

According to (9) and (10), the corresponding time-domain sensing channel matrix $\tilde{\mathbf{G}}(\tau, t)$ can be written as

$$
\begin{aligned}
\tilde{\mathbf{G}}(\tau, t) &= \tilde{\beta}_q e^{-j2\pi f_c^{\mathrm{BS}}\left(\tau_q^{\mathrm{BS},T}+\tau_q^{\mathrm{BS},R}+\frac{2(D_q-v_q t)}{c}\right)}\delta\Big(\tau-\tau_q^{\mathrm{BS},T}\\
&\quad -\tau_q^{\mathrm{BS},R}-\frac{2(D_q-v_q t)}{c}\Big)\\
&= \tilde{\beta}_q e^{-j2\pi f_c^{\mathrm{BS}}\tau_q}e^{-j2\pi f_c^{\mathrm{BS}}\left(\tau_q^{\mathrm{BS},T}+\tau_q^{\mathrm{BS},R}\right)}e^{j2\pi\nu_q t}\\
&\quad \times\delta\Big(\tau-\tau_q^{\mathrm{BS},T}-\tau_q^{\mathrm{BS},R}-\tau_q+\frac{2v_q t}{c}\Big)\\
&= \beta_q e^{j2\pi\nu_q t}e^{-j2\pi f_c^{\mathrm{BS}}\left(\tau_q^{\mathrm{BS},T}+\tau_q^{\mathrm{BS},R}\right)}\delta\big(\tau-\tau_q^{\mathrm{BS},T}\\
&\quad -\tau_q^{\mathrm{BS},R}-\tau_q\big),
\end{aligned}
\tag{11}
$$

where $\tau_q^{\mathrm{BS},T}$ and $\tau_q^{\mathrm{BS},R}$ are equal to $\frac{d(n_{\mathrm{BS}}^T-1)\sin\phi_q}{c}$ and $\frac{d(n_{\mathrm{BS}}^R-1)\sin\theta_q}{c}$, respectively. $\tau_q=\frac{2D_q}{c}$ denotes the two-way time delay of the q-th target, and $\nu_q=f_c^{\mathrm{BS}}\frac{2v_q}{c}$ represents the Doppler shift of the q-th target. The last equality holds since $\beta_q=\tilde{\beta}_q e^{-j2\pi f_c^{\mathrm{BS}}\tau_q}$, which is the equivalent reflection coefficient of the q-th target, and $v_q\ll c$ indicating that the relative radial velocity v_q of the q-th target is much smaller than the light speed c [27]. Consequently, the frequency-domain sensing channel matrix $\tilde{\mathbf{G}}(f, t)$ can be obtained by performing the Fourier transform on the variable τ of (11), given by

$$
\begin{aligned}
\tilde{\mathbf{G}}(f, t) &= \beta_q e^{j2\pi\nu_q t}e^{-j2\pi f_c^{\mathrm{BS}}\left(\tau_q^{\mathrm{BS},T}+\tau_q^{\mathrm{BS},R}\right)}e^{-j2\pi f\tau_q}\\
&\quad \times e^{-j2\pi f\left(\tau_q^{\mathrm{BS},T}+\tau_q^{\mathrm{BS},R}\right)}\\
&= \beta_q e^{-j2\pi(f+f_c^{\mathrm{BS}})\tau_q^{\mathrm{BS},T}}e^{-j2\pi(f+f_c^{\mathrm{BS}})\tau_q^{\mathrm{BS},R}}e^{-j2\pi f\tau_q}\\
&\quad \times e^{j2\pi\nu_q t}.
\end{aligned}
\tag{12}
$$

Ignoring the beam squint effects on antennas and combining all the elements from the BS transmitted and received antennas, the q-th target's frequency-domain sensing channel matrix $\mathbf{G}_q(f, t)$ can be written as

$$
\mathbf{G}_q(f, t) = \beta_q e^{-j2\pi f\tau_q}\mathbf{a}_{\mathrm{BS,R}}(\theta_q)\mathbf{a}_{\mathrm{BS,T}}^T(\phi_q)e^{j2\pi\nu_q t}, \tag{13}
$$

where $\mathbf{a}_{\mathrm{BS,R}}(\theta_q)$ and $\mathbf{a}_{\mathrm{BS,T}}(\phi_q)$ are the BS received and transmitted array steering vectors, given by

$$
\mathbf{a}_{\mathrm{BS,R}}(\theta_q)=\left[1, e^{-j2\pi\frac{d}{\lambda_c^{\mathrm{BS}}}\sin\theta_q}, \ldots, e^{-j2\pi\frac{d(N_{\mathrm{BS}}-1)}{\lambda_c^{\mathrm{BS}}}\sin\theta_q}\right]^T,
\tag{14}
$$

and

$$
\mathbf{a}_{\mathrm{BS,T}}(\phi_q)=\left[1, e^{-j2\pi\frac{d}{\lambda_c^{\mathrm{BS}}}\sin\phi_q}, \ldots, e^{-j2\pi\frac{d(N_{\mathrm{BS}}-1)}{\lambda_c^{\mathrm{BS}}}\sin\phi_q}\right]^T,
\tag{15}
$$

respectively. It is worth noting that the AoD ϕ_q and AoA θ_q of the q-th target are equal, i.e., $\phi_q=\theta_q$, since the transmit and receive antennas of radar are colocated. Consequently, the sensing channel $\mathbf{G}_q^k(n)$ can be obtained by executing the same process as acquiring the communication channel $\mathbf{H}_u^k(n)$, which can be presented as

$$
\begin{aligned}
\mathbf{G}_q^k(n) &= \mathbf{G}_q\left(\frac{kf_s}{K}, n(K+N_{CP})T_s\right)\\
&= \beta_q e^{-j2\pi\tau_q f_s\frac{k}{K}}\mathbf{a}_{\mathrm{BS,R}}(\theta_q)\mathbf{a}_{\mathrm{BS,T}}^T(\phi_q)e^{j2\pi\nu_q n(K+N_{CP})T_s}.
\end{aligned}
\tag{16}
$$

B. Signal Model

The received signals $\boldsymbol{y}^k(n)$ at the FD BS are divided into two parts, namely, the uplink communication signals $\boldsymbol{y}_c^k(n)$ and the echo signals of the downlink ISAC signals $\boldsymbol{y}_e^k(n)$, which can be expressed as[2]

$$
\boldsymbol{y}^k(n) = \boldsymbol{y}_c^k(n)+\boldsymbol{y}_e^k(n)+\boldsymbol{n}^k(n), \tag{17}
$$

where $\boldsymbol{n}^k(n)\in\mathbb{C}^{N_S^{\mathrm{BS},R}\times 1}$ represents the equivalent noise, modeled as additive white Gaussian noise with $\boldsymbol{n}^k(n)\sim\mathcal{CN}(0,\sigma^2\mathbf{I})$. Without loss of generality, it is assumed that $N_S^{\mathrm{BS},R}=M_{\mathrm{BS}}$.

For the uplink communication link, the u-th uplink UE sends the training communication symbol sequence $\boldsymbol{s}_u^k(n)\in\mathbb{C}^{N_S^{\mathrm{UE}}\times 1}$ at the n-th frame and k-th subcarrier, where the corresponding training precoded communication signal $\mathbf{f}_u^k(n)$ can be expressed by

$$
\mathbf{f}_u^k(n)=\mathbf{F}_{\mathrm{RF},u}^{\mathrm{UE}}\mathbf{F}_{\mathrm{BB},u}^k(n)\boldsymbol{s}_u^k(n), \tag{18}
$$

where $\mathbf{F}_{\mathrm{RF},u}^{\mathrm{UE}}\in\mathbb{C}^{N_{\mathrm{UE}}\times M_{\mathrm{UE}}}$ and $\mathbf{F}_{\mathrm{BB},u}^k(n)\in\mathbb{C}^{M_{\mathrm{UE}}\times N_S^{\mathrm{UE}}}$ are the u-th uplink UE's analog RF precoder and digital baseband precoder at the n-th frame and the k-th subcarrier, respectively. This training precoded communication signal is processed by the analog combiner $\mathbf{W}_{\mathrm{RF}}^{\mathrm{BS}}\in\mathbb{C}^{N_{\mathrm{BS}}\times M_{\mathrm{BS}}}$ and digital combiner $\mathbf{W}_{\mathrm{BB}}^k\in\mathbb{C}^{M_{\mathrm{BS}}\times M_{\mathrm{BS}}}$ at the BS. Therefore, the final received communication signal $\boldsymbol{y}_c^k(n)\in\mathbb{C}^{M_{\mathrm{BS}}\times 1}$ can be presented by

$$
\boldsymbol{y}_c^k(n)=\sum_{u=1}^{U}\left(\mathbf{W}_{\mathrm{BB,RF}}^k\right)^H\mathbf{H}_u^k(n)\mathbf{f}_u^k(n), \tag{19}
$$

where $\mathbf{H}_u^k(n)\in\mathbb{C}^{N_{\mathrm{BS}}\times N_{\mathrm{UE}}}$ is the communication channel matrix, and $\mathbf{W}_{\mathrm{BB,RF}}^k=\mathbf{W}_{\mathrm{RF}}^{\mathrm{BS}}\mathbf{W}_{\mathrm{BB}}^k$ is the equivalent combiner.[3]

For the downlink ISAC link, the ISAC symbol sequence $\boldsymbol{s}^k(n)\in\mathbb{C}^{N_S^{\mathrm{BS},T}\times 1}$ is sent, and the corresponding training precoded ISAC signal $\mathbf{f}_q^k(n)$ can be expressed as

$$
\mathbf{f}_q^k(n)=\mathbf{F}_{\mathrm{RF}}^{\mathrm{BS}}\mathbf{F}_{\mathrm{BB}}^k(n)\boldsymbol{s}^k(n), \tag{20}
$$

where $\mathbf{F}_{\mathrm{RF}}^{\mathrm{BS}}\in\mathbb{C}^{N_{\mathrm{BS}}\times M_{\mathrm{BS}}}$ and $\mathbf{F}_{\mathrm{BB}}^k(n)\in\mathbb{C}^{M_{\mathrm{BS}}\times N_S^{\mathrm{BS},T}}$ are the analog RF precoder and digital baseband precoder at

---

[2]The self-interference (SI) signal caused by the FD mode of the BS can be suppressed by the advanced self-interference cancellation (SIC) techniques, including antenna isolation, analog cancellation, and digital cancellation, where -70dB SI attenuation can be achieved by the antenna isolation technique [28], and -50dB SI attenuation can be obtained by the digital cancellation technique [29], respectively. Consequently, the total SI suppression can reach around -130dB [29] in a well-designed SIC system. Therefore the SI signal can be eliminated and ignored in $\boldsymbol{y}^k(n)$.

[3]The time indices of the digital combiner $\mathbf{W}_{\mathrm{BB}}^k$ and the equivalent combiner $\mathbf{W}_{\mathrm{BB,RF}}^k$ are omitted, as in the considered scenario, the implementation takes place at the ISAC BS, where these combiners can be treated as known quantities, regardless of potential time variations.

the BS, respectively. Once reflected by the q-th surrounding target, the final received echo signal $\boldsymbol{y}_e^k(n) \in \mathbb{C}^{M_{\mathrm{BS}} \times 1}$ can be obtained and handled by the equivalent combiner $\mathbf{W}_{\mathrm{BB,RF}}^k$, given by

$$\boldsymbol{y}_e^k(n) = \sum_{q=1}^{Q} \left(\mathbf{W}_{\mathrm{BB,RF}}^k\right)^H \mathbf{G}_q^k(n) \mathbf{f}_q^k(n), \tag{21}$$

where $\mathbf{G}_q^k(n) \in \mathbb{C}^{N_{\mathrm{BS}} \times N_{\mathrm{BS}}}$ is the sensing channel matrix.

III. UNIFIED TENSOR-BASED MODELING AND ANALYSIS FOR COMMUNICATION CHANNEL AND SENSING TARGETS PARAMETER ESTIMATION

In this section, a unified tensor-based channel for communication and sensing is modeled, and the uniqueness condition of the CPD problem is analyzed, which can ensure the decomposed factor matrices contain all the information about the unknown parameters.

A. Unified Tensor-Based Modeling for Communication Channel and Sensing Targets Parameter Estimation

By substituting (8), (16), (19), and (21) into (17), the ultimate signal received by the BS can be expressed by

$$\begin{aligned} \boldsymbol{y}^k(n) = & \sum_{u=1}^{U} \left(\mathbf{W}_{\mathrm{BB,RF}}^k\right)^H \Big(\sum_{l=1}^{\tilde{L}_c^u} \alpha_l e^{-j2\pi\tau_l f_s \frac{k}{K}} \mathbf{a}_{\mathrm{BS}}(\theta_l) \mathbf{a}_{\mathrm{UE}}^T(\phi_l) \\ & \times e^{j2\pi\nu_l n(K+N_{CP})T_s} \Big) \mathbf{f}_u^k(n) \\ & + \sum_{q=1}^{Q} \left(\mathbf{W}_{\mathrm{BB,RF}}^k\right)^H \beta_q e^{-j2\pi\tau_q f_s \frac{k}{K}} \mathbf{a}_{\mathrm{BS,R}}(\theta_q) \mathbf{a}_{\mathrm{BS,T}}^T(\phi_q) \\ & \times e^{j2\pi\nu_q n(K+N_{CP})T_s} \mathbf{f}_q^k(n) + \boldsymbol{n}^k(n). \end{aligned} \tag{22}$$

Subsequently, the unified form of $\boldsymbol{y}^k(n)$ can be obtained as follows

$$\begin{aligned} \boldsymbol{y}^k(n) = & \sum_{l_u=1}^{L_c} \left(\mathbf{W}_{\mathrm{BB,RF}}^k\right)^H \alpha_{l_u} e^{-j2\pi\tau_{l_u} f_s \frac{k}{K}} \mathbf{a}_{\mathrm{BS}}(\theta_{l_u}) \mathbf{a}_{\mathrm{UE}}^T(\phi_{l_u}) \\ & \times e^{j2\pi\nu_{l_u} n(K+N_{CP})T_s} \mathbf{f}_{l_u}^k(n) + \\ & \sum_{l_q=1}^{L_e} \left(\mathbf{W}_{\mathrm{BB,RF}}^k\right)^H \beta_{l_q} e^{-j2\pi\tau_{l_q} f_s \frac{k}{K}} \mathbf{a}_{\mathrm{BS,R}}(\theta_{l_q}) \mathbf{a}_{\mathrm{BS,T}}^T(\phi_{l_q}) \\ & \times e^{j2\pi\nu_{l_q} n(K+N_{CP})T_s} \mathbf{f}_{l_q}^k(n) + \boldsymbol{n}^k(n) \\ = & \sum_{l_a=1}^{L} \left(\mathbf{W}_{\mathrm{BB,RF}}^k\right)^H \gamma_{l_a} e^{-j2\pi\tau_{l_a} f_s \frac{k}{K}} \mathbf{a}_{\mathrm{R}}(\theta_{l_a}) \mathbf{a}_{\mathrm{T}}^T(\phi_{l_a}) \\ & \times e^{j2\pi\nu_{l_a} n(K+N_{CP})T_s} \mathbf{f}_{l_a}^k(n) + \boldsymbol{n}^k(n), \end{aligned} \tag{23}$$

where $L = L_c + L_e$ represents the number of the entire paths, and l_a is the path index. γ_{l_a} and τ_{l_a} denote the unified path gain and time delay of the l_a-th path, respectively. $\mathbf{a}_{\mathrm{R}}(\theta_{l_a})$ and $\mathbf{a}_{\mathrm{T}}(\phi_{l_a})$ are the unified received and transmitted array steering vectors of the l_a-th path, respectively. ν_{l_a} and $\mathbf{f}_{l_a}^k(n)$ denote the unified Doppler shift and training precoded signal, respectively. Consequently, by employing the frequency-flat beam training scheme in [17], i.e., $\mathbf{W}_{\mathrm{BB,RF}}^k = \mathbf{W}_{\mathrm{BB,RF}} = \mathbf{W}$

and $\mathbf{f}_{l_a}^k(n) = \mathbf{f}_{l_a}(n)$, the received signals $\mathbf{Y}^k$ stacking from the N frames can be expressed as

$$\mathbf{Y}^k = \sum_{l_a=1}^{L} e^{-j2\pi\tau_{l_a} f_s \frac{k}{K}} \tilde{\mathbf{a}}_{\mathrm{R}}(\gamma_{l_a}, \theta_{l_a}) \tilde{\mathbf{a}}_{\mathrm{T}}^T(\phi_{l_a}) \boldsymbol{\Gamma}(\nu_{l_a}) + \boldsymbol{N}^k, \tag{24}$$

where $\tilde{\mathbf{a}}_{\mathrm{R}}(\gamma_{l_a}, \theta_{l_a}) = \gamma_{l_a} \mathbf{W}^H \mathbf{a}_{\mathrm{R}}(\theta_{l_a}) \in \mathbb{C}^{M_{\mathrm{BS}} \times 1}$ and $\tilde{\mathbf{a}}_{\mathrm{T}}(\phi_{l_a}) = \mathbf{F}_{l_a}^T \mathbf{a}_{\mathrm{T}}(\phi_{l_a}) \in \mathbb{C}^{N \times 1}$ are the equivalent received and transmitted array steering vectors of the l_a-th path, respectively, and $\mathbf{F}_{l_a} = [\mathbf{f}_{l_a}(1), \ldots, \mathbf{f}_{l_a}(N)]$ denotes the unified training precoded signal stacking from the N frames. $\boldsymbol{\Gamma}(\nu_{l_a}) = diag([e^{j2\pi\nu_{l_a}(K+N_{CP})T_s}, \ldots, e^{j2\pi\nu_{l_a}N(K+N_{CP})T_s}]) \in \mathbb{C}^{N \times N}$ and $\boldsymbol{N}^k = [\boldsymbol{n}^k(1), \ldots, \boldsymbol{n}^k(N)] \in \mathbb{C}^{M_{\mathrm{BS}} \times N}$ denote the Doppler shift diagonal matrix and noise matrix, respectively. In addition, $\mathbf{Y}^k = [\boldsymbol{y}^k(1), \ldots, \boldsymbol{y}^k(N)] \in \mathbb{C}^{M_{\mathrm{BS}} \times N}$ contains the entire received communication and echo signals at the k-th subcarrier. Subsequently, the corresponding third-order tensor $\boldsymbol{\mathcal{Y}} \in \mathbb{C}^{M_{\mathrm{BS}} \times N \times \overline{K}}$ satisfying the given CPD format [30] can be acquired by stacking the entire communication and echo signals of $\overline{K}$ training subcarriers, given by

$$\begin{aligned} \boldsymbol{\mathcal{Y}} &= \left[\!\left[\mathbf{A}^{(1)}, \mathbf{A}^{(2)}, \mathbf{A}^{(3)}\right]\!\right] + \boldsymbol{\mathcal{N}} \\ &= \sum_{l_a=1}^{L} \tilde{\mathbf{a}}_{\mathrm{R}}(\gamma_{l_a}, \theta_{l_a}) \circ \tilde{\mathbf{b}}_{\mathrm{T}}(\phi_{l_a}, \nu_{l_a}) \circ \tilde{\mathbf{c}}(\tau_{l_a}) + \boldsymbol{\mathcal{N}}, \end{aligned} \tag{25}$$

where $\boldsymbol{\mathcal{N}} \in \mathbb{C}^{M_{\mathrm{BS}} \times N \times \overline{K}}$ is the unified noise tensor, and the three factor matrices $\mathbf{A}^{(1)}$, $\mathbf{A}^{(2)}$ and $\mathbf{A}^{(3)}$ can be written as

$$\mathbf{A}^{(1)} = [\tilde{\mathbf{a}}_{\mathrm{R}}(\gamma_1, \theta_1), \ldots, \tilde{\mathbf{a}}_{\mathrm{R}}(\gamma_L, \theta_L)] \in \mathbb{C}^{M_{\mathrm{BS}} \times L}, \tag{26}$$

$$\mathbf{A}^{(2)} = \left[\tilde{\mathbf{b}}_{\mathrm{T}}(\phi_1, \nu_1), \ldots, \tilde{\mathbf{b}}_{\mathrm{T}}(\phi_L, \nu_L)\right] \in \mathbb{C}^{N \times L}, \tag{27}$$

$$\mathbf{A}^{(3)} = [\tilde{\mathbf{c}}(\tau_1), \ldots, \tilde{\mathbf{c}}(\tau_L)] \in \mathbb{C}^{\overline{K} \times L}, \tag{28}$$

where $\tilde{\mathbf{b}}_{\mathrm{T}}(\phi_{l_a}, \nu_{l_a}) = \boldsymbol{\Gamma}(\nu_{l_a}) \tilde{\mathbf{a}}_{\mathrm{T}}(\phi_{l_a})$ denotes the unified transmitted array steering vector of the l_a-th path with the Doppler shift ν_{l_a}, and $\tilde{\mathbf{c}}(\tau_{l_a}) = [e^{-j2\pi\tau_{l_a} f_s \frac{k}{K}}]_{k=1}^{\overline{K}}$. It is worth noting that the objective of this paper is to estimate the unknown parameters $\{\gamma_{l_a}, \theta_{l_a}, \phi_{l_a}, \nu_{l_a}, \tau_{l_a}\}_{l_a=1}^{L}$ from $\boldsymbol{\mathcal{Y}}$, which can be mathematically expressed as

$$\underset{\mathbf{A}^{(1)}, \mathbf{A}^{(2)}, \mathbf{A}^{(3)}}{\text{minimize}} \left\| \boldsymbol{\mathcal{Y}} - \sum_{l_a=1}^{L} \tilde{\mathbf{a}}_{\mathrm{R}}(\gamma_{l_a}, \theta_{l_a}) \circ \tilde{\mathbf{b}}_{\mathrm{T}}(\phi_{l_a}, \nu_{l_a}) \circ \tilde{\mathbf{c}}(\tau_{l_a}) \right\|_F^2. \tag{29}$$

B. Uniqueness Property Analysis for Unified Tensor-Based Model

For the CPD problem (29), the analysis of the uniqueness condition is necessary, which is used to guarantee the communication channel and sensing target parameters can be uniquely determined with the decomposed factor matrices with the entire information of unknown parameters. In particular, the sufficient condition for the uniqueness of the CPD in the generic case is given in **Lemma 1** as follows [31].

Lemma 1: Considering the three factor matrices $\mathbf{A}^{(1)} \in \mathbb{C}^{M_{\mathrm{BS}} \times L}$, $\mathbf{A}^{(2)} \in \mathbb{C}^{N \times L}$, and $\mathbf{A}^{(3)} \in \mathbb{C}^{\overline{K} \times L}$ of the tensor

$\boldsymbol{\mathcal{Y}} \in \mathbb{C}^{M_{\mathrm{BS}} \times N \times \overline{K}}$ with rank L, the uniqueness of the CPD of $\boldsymbol{\mathcal{Y}}$ can be proved if the Kruskal's condition $\mathrm{k}(\mathbf{A}_{(1)}) + \mathrm{k}(\mathbf{A}_{(2)}) + \mathrm{k}(\mathbf{A}_{(3)}) \geq 2L + 2$ is satisfied. Specifically, this uniqueness condition can be transformed as

$$\min(M_{\mathrm{BS}}, L) + \min(N, L) + \min(\overline{K}, L) \geq 2L + 2, \quad (30)$$

when these three factor matrices' elements are taken from probability density functions that are absolutely continuous and have probability one [32].

According to (30), the maximum number L of paths can be determined by the given number of the received RF chains, frames, and training subcarriers. Particularly, it is worth noting that L can be further expanded due to the algebraic structures of $\mathbf{A}^{(3)}$, i.e., the Vandermonde structure. Therefore, the relaxed uniqueness condition is given in **Lemma 2** as follows [33].

Lemma 2: Considering the three factor matrices $\mathbf{A}^{(1)} \in \mathbb{C}^{M_{\mathrm{BS}} \times L}$, $\mathbf{A}^{(2)} \in \mathbb{C}^{N \times L}$, and $\mathbf{A}^{(3)} \in \mathbb{C}^{\overline{K} \times L}$ of the tensor $\boldsymbol{\mathcal{Y}} \in \mathbb{C}^{M_{\mathrm{BS}} \times N \times \overline{K}}$ with rank L, where $\mathbf{A}^{(3)}$ is the Vandermonde structure, the uniqueness of the CPD of $\boldsymbol{\mathcal{Y}}$ can be guaranteed if the following condition is satisfied, given by

$$\begin{cases} \mathrm{rank}\left(\left[\mathbf{A}^{(3)}\right]_{1:L_3} \odot \mathbf{A}^{(1)}\right) = L, \\ \mathrm{rank}\left(\left[\mathbf{A}^{(3)}\right]_{1:(K_3-1)} \odot \mathbf{A}^{(2)}\right) = L, \end{cases} \quad (31)$$

where $L_3 + K_3 - 1 = \overline{K}$. Specifically, this uniqueness condition can be transformed into the following form, given by

$$\min\left(N(K_3 - 1), M_{\mathrm{BS}} L_3\right) \geq L, \quad (32)$$

when these three factor matrices' elements are taken from probability density functions that are absolutely continuous and have probability one [32].

According to (32), the maximum number L of paths can be further enlarged by improving the number of frames, training subcarriers, or RF chains, which indicates that the communication channel and sensing target parameters of more paths can be estimated more accurately.

IV. CPD-BASED UNIFIED PARAMETER ESTIMATION ALGORITHM

In this section, a two-stage CPD-based unified communication channel and sensing targets parameter estimation algorithm is proposed. In the first stage, the algorithm to estimate factor matrices from the observation tensor $\boldsymbol{\mathcal{Y}}$ is provided, and the algorithm to extract the parameters $\{\gamma_{l_a}, \theta_{l_a}, \phi_{l_a}, \nu_{l_a}, \tau_{l_a}\}_{l_a=1}^{L}$ of the communication channel and sensing targets from the estimated factor matrices is proposed in the second stage.

A. Factor Matrix Estimation

For the received observation tensor $\boldsymbol{\mathcal{Y}}$, one of the most traditional algorithms to estimate the factor matrices is the alternating least squares (ALS)-based algorithm [34]. By using the ALS-based algorithm to estimate the factor matrices $\{\mathbf{A}^{(1)}, \mathbf{A}^{(2)}, \mathbf{A}^{(3)}\}$, the initial value of the estimated factor matrices $\{\hat{\mathbf{A}}^{(1)}, \hat{\mathbf{A}}^{(2)}, \hat{\mathbf{A}}^{(3)}\}$ should be randomly generated first, and then the estimated factor matrices can be obtained by

alternatively updating one factor matrix and fixing the other two factor matrices until convergence, the process of which can be expressed as follows

$$\mathbf{A}_{i+1}^{(1)} = \arg\min_{\mathbf{A}^{(1)}} \left\| \mathbf{Y}_{(1)}^{T} - \left(\mathbf{A}_i^{(3)} \odot \mathbf{A}_i^{(2)}\right)\left(\mathbf{A}_i^{(1)}\right)^{T} \right\|_F^2, \quad (33)$$

$$\mathbf{A}_{i+1}^{(2)} = \arg\min_{\mathbf{A}^{(2)}} \left\| \mathbf{Y}_{(2)}^{T} - \left(\mathbf{A}_i^{(3)} \odot \mathbf{A}_i^{(1)}\right)\left(\mathbf{A}_i^{(2)}\right)^{T} \right\|_F^2, \quad (34)$$

$$\mathbf{A}_{i+1}^{(3)} = \arg\min_{\mathbf{A}^{(3)}} \left\| \mathbf{Y}_{(3)}^{T} - \left(\mathbf{A}_i^{(2)} \odot \mathbf{A}_i^{(1)}\right)\left(\mathbf{A}_i^{(3)}\right)^{T} \right\|_F^2, \quad (35)$$

where $\mathbf{A}_m^{(n)}, m \in \{i, i+1\}, n \in \{1, 2, 3\}$ denotes the n-th factor matrix in the m-th iteration. Although the above algorithm is efficient and mature for estimating factor matrices, there are four limitations: 1) Failure to converge at low signal-to-noise ratios (SNRs); 2) The convergence speed is unstable; 3) A local optimal solution may be obtained; 4) The structural characteristics of the factor matrix are not utilized, thus making it impossible to estimate the maximum number of path parameters from the estimated factor matrices. Therefore, a matrix subspace-based method using the Vandermonde structure characteristics of $\mathbf{A}^{(3)}$ is proposed. Specifically, considering $\mathbf{Y}_{(1)}^{T} = (\mathbf{A}^{(3)} \odot \mathbf{A}^{(2)})(\mathbf{A}^{(1)})^{T} + \mathbf{N}_{(1)}^{T}$, a cyclic selection matrix $\mathbf{J}_l = \left[\mathbf{0}_{K_3 \times (l-1)} \ \mathbf{I}_{K_3} \ \mathbf{0}_{K_3 \times (L_3-l)}\right]$ is used to expand the dimension of $\mathbf{Y}_{(1)}$ for obtaining $\mathbf{Y}_{(1)}^{e}$ as follows

$$\begin{aligned} \mathbf{Y}_{(1)}^{e} &= \left[(\mathbf{J}_1 \otimes \mathbf{I}_N)\mathbf{Y}_{(1)}^{T}, \ldots, (\mathbf{J}_{L_3} \otimes \mathbf{I}_N)\mathbf{Y}_{(1)}^{T}\right] \\ &= \left(\left[\mathbf{A}^{(3)}\right]_{1:K_3} \odot \mathbf{A}^{(2)}\right)\left(\left[\mathbf{A}^{(3)}\right]_{1:L_3} \odot \mathbf{A}^{(1)}\right)^{T} + \mathbf{N}_{(1)}^{e}, \end{aligned} \quad (36)$$

where $\mathbf{N}_{(1)}^{e} \in \mathbb{C}^{K_3 N \times L_3 M_{\mathrm{BS}}}$ is the noise matrix. Here, the last equality holds due to $\mathbf{A}^{(3)}$ has the Vandermonde structure [33]. Consequently, one can refer to [19] and use linear algebra, such as the truncated singular value decomposition (SVD) and the eigenvalue decomposition (EVD), to further estimate the factor matrices. Specifically, the truncated SVD is performed on $\mathbf{Y}_{(1)}^{e}$, and the decomposition result can be expressed as $\mathbf{Y}_{(1)}^{e} = \mathbf{U} \circ \mathbf{V}^{H}$. After extracting the submatrices $\mathbf{U}_1 = [\mathbf{U}]_{1:(K_3-1)N,:} \in \mathbb{C}^{(K_3-1)N \times L}$ and $\mathbf{U}_2 = [\mathbf{U}]_{N+1:K_3 N,:} \in \mathbb{C}^{(K_3-1)N \times L}$ from the left singular vector $\mathbf{U}$, the EVD can be performed to decompose the matrix $\mathbf{U}_1^{\dagger} \mathbf{U}_2$, given by

$$\mathbf{U}_1^{\dagger} \mathbf{U}_2 = \mathbf{M} \mathbf{Z} \mathbf{M}^{-1}, \quad (37)$$

where $\mathbf{M} \in \mathbb{C}^{L \times L}$ is the left eigenvector, and the diagonal matrix $\mathbf{Z} \in \mathbb{C}^{L \times L}$ contains the information of the equivalent time delays on its diagonal elements $\{z_l = e^{-j2\pi\tau_l f_s \frac{1}{K}}\}_{l=1}^{L}$. Therefore, the l_a-th column of $\hat{\mathbf{A}}^{(3)}$ can be reconstructed as

$$\hat{\mathbf{a}}_{l_a}^{(3)} = \left[z_{l_a}, z_{l_a}^2, \ldots, z_{l_a}^{\overline{K}}\right]^{T}. \quad (38)$$

Sequentially, the l_a-th column of the factor matrices $\hat{\mathbf{A}}^{(2)}$ and $\hat{\mathbf{A}}^{(1)}$ can be acquired, given by

$$\hat{\mathbf{a}}_{l_a}^{(2)} = \left(\frac{\left[\hat{\mathbf{a}}_{l_a}^{(3)} \right]_{1:K_3}^*}{K_3} \otimes \mathbf{I}_N \right) \mathbf{U}[\mathbf{M}]_{:,l_a}, \quad (39)$$

and

$$\hat{\mathbf{a}}_{l_a}^{(1)} = \left(\frac{\left[\hat{\mathbf{a}}_{l_a}^{(3)} \right]_{1:L_3}^*}{L_3} \otimes \mathbf{I}_{M_{\text{BS}}} \right) \mathbf{V}^* \mathbf{\Sigma} \left[\mathbf{M}^{-T} \right]_{:,l_a}, \quad (40)$$

respectively. According to (38), (39), and (40), we have

$$\hat{\mathbf{A}}^{(n)} = \mathbf{A}^{(n)} \mathbf{\Pi} \mathbf{\Delta}_n + \mathbf{E}_n, \quad (41)$$

where $n \in \{1, 2, 3\}$, $\mathbf{\Pi} \in \mathbb{C}^{L \times L}$ denotes the unknown permutation matrix, $\mathbf{\Delta}_n$ is the unknown diagonal matrix satisfying $\mathbf{\Delta}_1 \mathbf{\Delta}_2 \mathbf{\Delta}_3 = \mathbf{I}_L$, and $\mathbf{E}_n$ represents the estimation errors of the factor matrices.

B. Path Parameter Estimation

According to (26) and (28), θ_{l_a} and τ_{l_a} can be extracted by a correlation-based scheme [17], where the estimated parameters $\hat{\theta}_{l_a}$ and $\hat{\tau}_{l_a}$ can be expressed as

$$\hat{\theta}_{l_a} = \arg \max_{\theta_{l_a}} \frac{\left| \left(\hat{\mathbf{a}}_{l_a}^{(1)} \right)^H \mathbf{W}^H \mathbf{a}_{\text{R}}(\theta_{l_a}) \right|^2}{\left\| \hat{\mathbf{a}}_{l_a}^{(1)} \right\|_2^2 \left\| \mathbf{W}^H \mathbf{a}_{\text{R}}(\theta_{l_a}) \right\|_2^2}, \quad (42)$$

$$\hat{\tau}_{l_a} = \arg \max_{\tau_{l_a}} \frac{\left| \left(\hat{\mathbf{a}}_{l_a}^{(3)} \right)^H \tilde{\mathbf{c}}(\tau_{l_a}) \right|^2}{\left\| \hat{\mathbf{a}}_{l_a}^{(3)} \right\|_2^2 \left\| \tilde{\mathbf{c}}(\tau_{l_a}) \right\|_2^2}, \quad (43)$$

respectively. By employing the one-dimensional search in the scope of θ_{l_a} and τ_{l_a}, respectively, the problems of (42) and (43) can be easily handled. Then, since the AoD and the Doppler shift are coupled, the joint estimation problem of estimating ϕ_{l_a} and ν_{l_a} can be presented as

$$\hat{\mathbf{D}} = \arg \min_{\mathbf{D}} \left\| \hat{\mathbf{a}}_{l_a}^{(2)} - \delta_{l_a} \mathbf{\Gamma}(\nu_{l_a}) \mathbf{F}_{l_a}^T \mathbf{a}_{\text{T}}(\phi_{l_a}) \right\|_2^2, \quad (44)$$

where $\hat{\mathbf{D}} = \{ \hat{\delta}_{l_a}, \hat{\nu}_{l_a}, \hat{\mathbf{F}}_{l_a}, \hat{\phi}_{l_a} \}$ is the estimated parameter set, and $\mathbf{D} = \{ \delta_{l_a}, \nu_{l_a}, \mathbf{F}_{l_a}, \phi_{l_a} \}$. δ_{l_a} and $\hat{\delta}_{l_a}$ are the l_a-th true and estimated diagonal elements of $\mathbf{\Delta}_2$, respectively. To solve this problem, a JAI-PCE algorithm is proposed, which consists of two stages, namely, initialization stage and estimation stage. In the initialization stage, the initial value of the estimated training precoded signal $\hat{\mathbf{F}}_{l_a}^{(0)}$ and the estimated AoD $\hat{\phi}_{l_a}^{(0)}$ can be acquired by employing the proposed correlation value-based two-dimensional search in the scope of $\mathbf{F}_{l_a}$ and ϕ_{l_a}, which can be expressed as

$$\{ \hat{\mathbf{F}}_{l_a}^{(0)}, \hat{\phi}_{l_a}^{(0)} \} = \arg \max_{\mathbf{F}_{l_a}, \phi_{l_a}} \frac{\left| \mathbf{a}_{\text{T}}^H(\phi_{l_a}) \mathbf{F}_{l_a}^* \hat{\mathbf{a}}_{l_a}^{(2)} \right|^2}{\left\| \mathbf{F}_{l_a}^T \mathbf{a}_{\text{T}}(\phi_{l_a}) \right\|_2^2}, \quad (45)$$

where $\frac{|\mathbf{a}_{\text{T}}^H(\phi_{l_a}) \mathbf{F}_{l_a}^* \hat{\mathbf{a}}_{l_a}^{(2)}|^2}{\|\mathbf{F}_{l_a}^T \mathbf{a}_{\text{T}}(\phi_{l_a})\|_2^2}$ is the correlation value. The combination of $\mathbf{F}_{l_a}$ and ϕ_{l_a} with the maximal correlation value can be selected by our proposed method. For inactive UEs, the order of magnitude of the correlation value is much smaller than that of active UEs and radar targets. Therefore, the total number of active UEs and radar targets can be determined by a given empirical threshold λ. Since the BS has all UEs' and targets' pilot information, it is easy to distinguish whether current path parameter belongs to an uplink UE or a radar target. In the estimation stage, $\hat{\delta}_{l_a}$, $\hat{\nu}_{l_a}$, $\hat{\mathbf{F}}_{l_a}$, and $\hat{\phi}_{l_a}$ can be obtained by alternating iterative optimization, given by

$$\hat{\delta}_{l_a}^{(i)} = \arg \min_{\delta_{l_a}} \left\| \hat{\mathbf{a}}_{l_a}^{(2)} - \delta_{l_a} \mathbf{\Gamma}\left(\hat{\nu}_{l_a}^{(i-1)} \right) \left(\hat{\mathbf{F}}_{l_a}^{(i-1)} \right)^T \mathbf{a}_{\text{T}}\left(\hat{\phi}_{l_a}^{(i-1)} \right) \right\|_2^2, \quad (46)$$

$$\hat{\nu}_{l_a}^{(i)} = \arg \min_{\nu_{l_a}} \left\| \hat{\mathbf{a}}_{l_a}^{(2)} - \hat{\delta}_{l_a}^{(i)} \mathbf{\Gamma}(\nu_{l_a}) \left(\hat{\mathbf{F}}_{l_a}^{(i-1)} \right)^T \mathbf{a}_{\text{T}}\left(\hat{\phi}_{l_a}^{(i-1)} \right) \right\|_2^2, \quad (47)$$

$$\hat{\mathbf{F}}_{l_a}^{(i)} = \arg \min_{\mathbf{F}_{l_a}} \left\| \left(\mathbf{\Gamma}(\hat{\nu}_{l_a}^{(i)}) \right)^{-1} \hat{\mathbf{a}}_{l_a}^{(2)} - \hat{\delta}_{l_a}^{(i)} (\mathbf{F}_{l_a})^T \mathbf{a}_{\text{T}}\left(\hat{\phi}_{l_a}^{(i-1)} \right) \right\|_2^2, \quad (48)$$

$$\hat{\phi}_{l_a}^{(i)} = \arg \min_{\phi_{l_a}} \left\| \left(\mathbf{\Gamma}(\hat{\nu}_{l_a}^{(i)}) \right)^{-1} \hat{\mathbf{a}}_{l_a}^{(2)} - \hat{\delta}_{l_a}^{(i)} \left(\hat{\mathbf{F}}_{l_a}^{(i)} \right)^T \mathbf{a}_{\text{T}}(\phi_{l_a}) \right\|_2^2. \quad (49)$$

To guarantee the convergence and effectiveness of alternating iterative optimization, the monotonicity of iterative steps (46)-(49) should be analyzed. Therefore, **Lemma 3** is proposed to prove the objective function of (44) can be solved effectively by utilizing iterative steps (46)-(49).

Lemma 3: The non-increasing characteristic of the objective function $g(\hat{\delta}_{l_a}^{(i-1)}, \hat{\nu}_{l_a}^{(i-1)}, \hat{\mathbf{F}}_{l_a}^{(i-1)}, \hat{\phi}_{l_a}^{(i-1)})$ of (44) can be guaranteed by utilizing the iterative steps (46)-(49), given by

$$g\left(\hat{\delta}_{l_a}^{(i-1)}, \hat{\nu}_{l_a}^{(i-1)}, \hat{\mathbf{F}}_{l_a}^{(i-1)}, \hat{\phi}_{l_a}^{(i-1)} \right)$$
$$\geq g\left(\hat{\delta}_{l_a}^{(i)}, \hat{\nu}_{l_a}^{(i)}, \hat{\mathbf{F}}_{l_a}^{(i)}, \hat{\phi}_{l_a}^{(i)} \right). \quad (50)$$

Proof 1: See Appendix A.

According to **Lemma 3**, the objective function of (44) can be guaranteed to be non-increasing. Since $g(\hat{\delta}_{l_a}^{(i)}, \hat{\nu}_{l_a}^{(i)}, \hat{\mathbf{F}}_{l_a}^{(i)}, \hat{\phi}_{l_a}^{(i)})$ has a lower bound of zero, the results of iterative update processes can be converged with the sufficient iterative number N_{I} [8]. To simplify the iterative update processes (46)-(49), **Lemma 4** is proposed.

Lemma 4: The simple forms of iterative update processes (46)-(49) can be represented as

$$\hat{\delta}_{l_a}^{(i)} = \frac{\mathbf{a}_{\text{T}}^H\left(\hat{\phi}_{l_a}^{(i-1)} \right) \left(\hat{\mathbf{F}}_{l_a}^{(i-1)} \right)^* \hat{\mathbf{\Gamma}}^{-1}\left(\hat{\nu}_{l_a}^{(i-1)} \right) \hat{\mathbf{a}}_{l_a}^{(2)}}{\left\| \left(\hat{\mathbf{F}}_{l_a}^{(i-1)} \right)^T \mathbf{a}_{\text{T}}\left(\hat{\phi}_{l_a}^{(i-1)} \right) \right\|_2^2}, \quad (51)$$

$$\hat{\nu}_{l_a}^{(i)} = \arg \max_{\nu_{l_a}} \sum_{n=1}^N \text{Re}\left(e^{j 2\pi \nu_{l_a} n (K + N_{CP}) T_s} \hat{\delta}_{l_a}^{(i)} \left[\hat{\mathbf{a}}_{l_a}^{(2)} \right]_{:,n}^* \right.$$
$$\left. \times \left(\hat{\mathbf{f}}_{l_a}^{(i-1)}(n) \right)^T \mathbf{a}_{\text{T}}\left(\hat{\phi}_{l_a}^{(i-1)} \right) \right), \quad (52)$$

$$\hat{\mathbf{F}}_{l_a}^{(i)} = \arg \max_{\mathbf{F}_{l_a}} \frac{\left| \mathbf{a}_{\text{T}}^H\left(\hat{\phi}_{l_a}^{(i-1)} \right) \mathbf{F}_{l_a}^* \hat{\mathbf{\Gamma}}^{-1}\left(\hat{\nu}_{l_a}^{(i)} \right) \hat{\mathbf{a}}_{l_a}^{(2)} \right|^2}{\left\| \mathbf{F}_{l_a}^T \mathbf{a}_{\text{T}}\left(\hat{\phi}_{l_a}^{(i-1)} \right) \right\|_2^2}, \quad (53)$$

Algorithm 1 Proposed JAI-PCE Algorithm

Input: The estimated factor matrix $\hat{\mathbf{A}}^{(2)}$, the whole unified training precoded signal $\mathbf{F}_{l_a}, l_a = 1, 2, \ldots, L$ and the number of iterations N_{I}.

Output: $\{\hat{\delta}_{l_a}\}_{l_a=1}^L$, $\{\hat{\nu}_{l_a}\}_{l_a=1}^L$, $\{\hat{\mathbf{F}}_{l_a}\}_{l_a=1}^L$, and $\{\hat{\phi}_{l_a}\}_{l_a=1}^L$.

1: **for** $l_a = 1, 2, \ldots, L$ **do**
2:    Obtain the initial values, i.e., $\hat{\mathbf{F}}_{l_a}^{(0)}$ and $\hat{\phi}_{l_a}^{(0)}$, according to (45).
3:    Let $\hat{\nu}_{l_a}^{(0)} = 0, l_a = 1, 2, \ldots, L$.
4:    **for** $i = 1, 2, \ldots, N_{\mathrm{I}}$ **do**
5:       Calculate $\hat{\delta}_{l_a}^{(i)}$ via (51).
6:       Calculate $\hat{\nu}_{l_a}^{(i)}$ via (52).
7:       Calculate $\hat{\mathbf{F}}_{l_a}^{(i)}$ via (53).
8:       Calculate $\hat{\phi}_{l_a}^{(i)}$ via (54).
9:    **end for**
10:    Acquire $\hat{\delta}_{l_a} = \hat{\delta}_{l_a}^{(N_{\mathrm{I}})}$, $\hat{\nu}_{l_a} = \hat{\nu}_{l_a}^{(N_{\mathrm{I}})}$, $\hat{\mathbf{F}}_{l_a} = \hat{\mathbf{F}}_{l_a}^{(N_{\mathrm{I}})}$, and $\hat{\phi}_{l_a} = \hat{\phi}_{l_a}^{(N_{\mathrm{I}})}$.
11: **end for**

$$\hat{\phi}_{l_a}^{(i)} = \arg\max_{\phi_{l_a}} \frac{\left| \mathbf{a}_{\mathrm{T}}^H(\phi_{l_a}) \left(\hat{\mathbf{F}}_{l_a}^{(i)}\right)^* \hat{\mathbf{\Gamma}}^{-1}\left(\hat{\nu}_{l_a}^{(i)}\right) \hat{\mathbf{a}}_{l_a}^{(2)} \right|^2}{\left\| \left(\hat{\mathbf{F}}_{l_a}^{(i)}\right)^T \mathbf{a}_{\mathrm{T}}(\phi_{l_a}) \right\|_2^2}, \quad (54)$$

respectively.

Proof 2: See Appendix B.

It is worth noting that (51) can be calculated directly, while (52), (53), and (54) can be solved by a one-dimensional search. The details of the proposed JAI-PCE algorithm is summarized in **Algorithm** 1.

After obtaining $\{\hat{\theta}_{l_a}\}_{l_a=1}^L$, $\{\hat{\tau}_{l_a}\}_{l_a=1}^L$, $\{\hat{\nu}_{l_a}\}_{l_a=1}^L$, $\{\hat{\mathbf{F}}_{l_a}\}_{l_a=1}^L$, and $\{\hat{\phi}_{l_a}\}_{l_a=1}^L$, the path gains $\{\hat{\gamma}_{l_a}\}_{l_a=1}^L$ can be estimated according to $\mathbf{\Delta}_1 \mathbf{\Delta}_2 \mathbf{\Delta}_3 = \mathbf{I}_L$ by utilizing LS estimators [35]. Specifically, $\{\hat{\gamma}_{l_a}\}_{l_a=1}^L$ can be given by

$$[\mathbf{\Delta}_2]_{l_a,l_a} = \left(\mathbf{\Gamma}(\hat{\nu}_{l_a})\hat{\mathbf{F}}_{l_a}^T \mathbf{a}_{\mathrm{T}}(\hat{\phi}_{l_a})\right)^\dagger \hat{\mathbf{a}}_{l_a}^{(2)}, \quad (55)$$

$$[\mathbf{\Delta}_3]_{l_a,l_a} = \left(\tilde{\mathbf{c}}(\hat{\tau}_{l_a})\right)^\dagger \hat{\mathbf{a}}_{l_a}^{(3)}, \quad (56)$$

$$\mathbf{\Delta}_1 = \mathbf{\Delta}_3^{-1} \mathbf{\Delta}_2^{-1}, \quad (57)$$

$$\hat{\gamma}_{l_a} = [\mathbf{\Delta}_1]_{l_a,l_a}^{-1} \left(\mathbf{W}^H \mathbf{a}_{\mathrm{R}}(\hat{\theta}_{l_a})\right)^\dagger \hat{\mathbf{a}}_{l_a}^{(1)}. \quad (58)$$

With the whole estimated channel parameters, the communication and radar channels can be reconstructed according to (8) and (16). The computational complexity of the proposed CPD-based unified parameter estimation algorithm is analyzed as follows. In the stage of factor matrix estimation, the expansion operation, i.e., (36) takes $\mathcal{O}(K_3 N L_3 M_{\mathrm{BS}} L)$; the SVD and EVD have the complexity $\mathcal{O}(K_3 N L_3^2 M_{\mathrm{BS}}^2)$ and $\mathcal{O}(L^3)$, respectively; the estimation of $\hat{\mathbf{A}}^{(2)}$ and $\hat{\mathbf{A}}^{(1)}$, i.e., (39) and (40) require $\mathcal{O}(K_3 N L)$ and $\mathcal{O}(L_3 M_{\mathrm{BS}} L)$, respectively. In the stage of path parameter estimation, the number of the searching grid points N_{g} is given, considering the involved one-dimensional search method. Thus, the complexity of calculating (42) and (43) are $\mathcal{O}(M_{\mathrm{BS}} N_{\mathrm{BS}} L N_{\mathrm{g}})$ and $\mathcal{O}(\overline{K} L N_{\mathrm{g}})$, respectively; (52), (53),

and (54) take $\mathcal{O}(NLN_{\mathrm{g}} N_{\mathrm{I}})$, $\mathcal{O}(NLN_{\mathrm{g}} N_{\mathrm{I}} \frac{(N_{\mathrm{BS}}+N_{\mathrm{UE}})}{2})$, and $\mathcal{O}(NLN_{\mathrm{g}} N_{\mathrm{I}} \frac{(N_{\mathrm{BS}}+N_{\mathrm{UE}})}{2})$, respectively; the complexity of the calculation of (55)-(58) is $\mathcal{O}((M_{\mathrm{BS}} + N + \overline{K})L)$. The complexity of the proposed algorithm increases with $\overline{K}$, M_{BS}, and N, as these resources expand the dimensions of $\mathcal{Y}$, which also increase the complexity of factor matrix and path parameter estimation. Since the search spaces of the estimated path parameters are influenced by L, N_{g}, N_{I}, N_{BS}, and N_{UE}, the complexity of the proposed algorithm grows as these parameters increase. In addition, the ALS-based algorithm [34] and the OMP algorithm [36] are selected as comparison schemes to verify the superiority of our proposed algorithm in this paper. For the ALS-based algorithm, the only difference from the proposed algorithm lies in the factor matrix estimation process, whose complexity is $\mathcal{O}(M_{\mathrm{BS}} N \overline{K} L + (M_{\mathrm{BS}} N + M_{\mathrm{BS}} \overline{K} + N\overline{K})L^2 + L^3)$. In the case that $K_3 = L_3 = \overline{K}$, the complexity of the proposed algorithm during the factor matrix estimation phase is $\mathcal{O}(M_{\mathrm{BS}}^2 N \overline{K}^3 + (M_{\mathrm{BS}} N \overline{K}^2 + N\overline{K} + M_{\mathrm{BS}} \overline{K})L + L^3)$, indicating that the proposed algorithm's complexity is primarily induced by $\overline{K}$, M_{BS}, and N. For the OMP algorithm, the complexity is given by $\mathcal{O}(M_{\mathrm{BS}} N \overline{K} L + N_{\mathrm{g}}^3)$.

V. SIMULATION RESULTS

In this section, simulation results are presented to verify the effectiveness of our proposed CPD-based joint AUD and ISAC parameter estimation. The whole number of uplink UEs is set as $U = 100$. The BS is equipped with $N_{\mathrm{BS}} = 64$ antennas and $M_{\mathrm{BS}} = 40$ RF chains, while the uplink UEs employ $N_{\mathrm{UE}} = 32$ antennas with $M_{\mathrm{UE}} = 1$ RF chain [8]. The carrier frequencies of the BS and uplink UEs are $f_c^{\mathrm{BS}} = f_c^{\mathrm{UE}} = 28$ GHz, and the system sampling rate is set to $f_s = 100$ MHz. The total number of frames is $N = 50$, and the total number of subcarriers is $K = 256$, where the total number of training subcarriers is $\overline{K} = 60$. It is assumed that the number of uplink UE multipaths is 3 and the number of radar target paths is 1. The unified path delay τ_{l_a} is uniformly generated between 0 and 320 ns, and the maximum unified velocity $[v_{l_a}]_{max}$ is 30 m/s. The unified AoA θ_{l_a} and AoD ϕ_{l_a} are randomly sampled from $[-\frac{\pi}{2}, \frac{\pi}{2}]$, and the unified path gain γ_{l_a} is distributed to $\mathcal{CN}(0,1)$ [18]. The SNRs $\frac{\|\mathcal{Y} - \mathcal{N}\|_F^2}{\|\mathcal{N}\|_F^2}$ are set from 0dB to 20dB. For the one-dimensional search and the two-dimensional search, the searching grid points is $N_{\mathrm{g}} = 320$ for all parameters, and the number of iterations is set to $N_{\mathrm{I}} = 30$ [8]. To characterize the accuracy of AUD, the active detection accuracy (ADA) is selected as the performance metric, given by

$$\mathrm{ADA} = \frac{\left[\hat{\mathbb{A}} \cap \mathbb{A}\right]_c}{[\mathbb{A}]_c}, \quad (59)$$

where $\hat{\mathbb{A}}$ and $\mathbb{A}$ are the estimated and true sets of active users, respectively. To characterize the estimation performance of the communication and sensing parameters, NMSE($\mathbf{H}$) is selected to evaluate the channel matrix estimation performance of active UEs. Additionally, NMSE($\boldsymbol{x}$) and RMSE($\boldsymbol{x}$) are
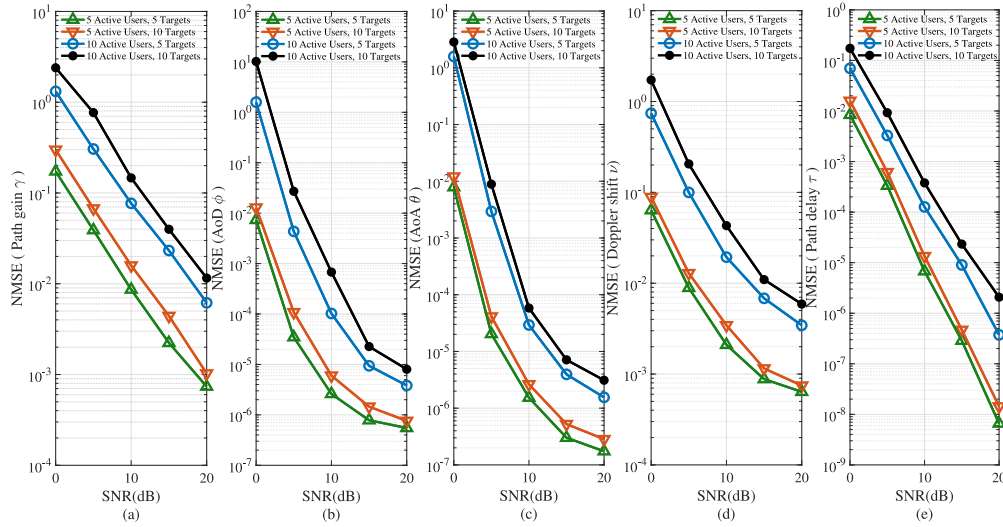
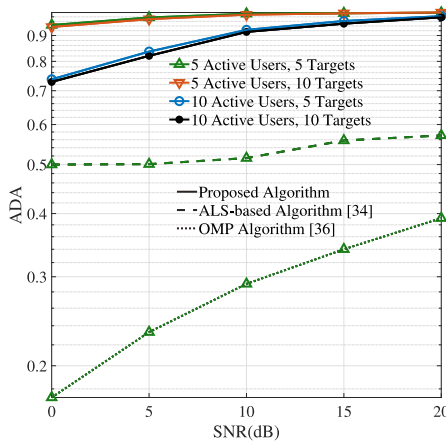Fig. 2. Path parameter estimation performance of proposed algorithm under various SNRs.

Fig. 3. ADA performance of different algorithms under various SNRs.

selected to evaluate the performance of the path parameter estimation and the radar target estimation, respectively, given by

$$\text{NMSE}(\mathbf{H}) = \frac{1}{\lambda UK} \sum_{u=1}^{\lambda U} \sum_{k=1}^{K} \frac{\left\| \hat{\mathbf{H}}_u^k(N) - \mathbf{H}_u^k(N) \right\|_F^2}{\left\| \mathbf{H}_u^k(N) \right\|_F^2}, \quad (60)$$

$$\text{NMSE}(\boldsymbol{x}) = \frac{1}{L} \sum_{l_a=1}^{L} \frac{\left| \hat{\boldsymbol{x}}_{l_a} - \boldsymbol{x}_{l_a} \right|^2}{\left| \boldsymbol{x}_{l_a} \right|^2}, \quad (61)$$

$$\text{RMSE}(\boldsymbol{x}) = \sqrt{\frac{1}{L_e} \sum_{l_a=1}^{L_e} \left| \hat{\boldsymbol{x}}_{l_a} - \boldsymbol{x}_{l_a} \right|^2}. \quad (62)$$

Fig. 2 shows the path parameter estimation performance under various SNRs. It can be seen from Fig. 2 that the normalized mean squared error (NMSE) performance of all path parameters improves with the increase of SNR. Due to the parameter coupling, the estimation performance curves of the three parameters of AoD ϕ, AoA θ, and Doppler shift ν corresponding to Fig. 2(b), Fig. 2(c), and Fig. 2(d) show a similar convergence trend, indicating that the solution

accuracy of the proposed CPD-based algorithm for these three parameters has reached its limit, while the performance curves of the corresponding gain γ and delay τ in Fig. 2(a) and Fig. 2(e) are still on a downward trend, indicating that better parameter estimation performance can be achieved by increasing the SNR. For gain γ and delay τ, when SNR = 20dB, the NMSE can reach the order of 10^{-3} and 10^{-8}, respectively, for 5 active users and 5 radar targets. For AoD ϕ, AoA θ, and Doppler shift ν, even for the case of 10 active users and 10 radar targets, the NMSE can reach the order of 10^{-5}, 10^{-5}, and 10^{-2}, respectively.

Fig. 3 illustrates the ADA performance under various SNRs. It can be observed that the performance of the ALS-based algorithm and the OMP algorithm both improve with the increase of SNR in the case of 5 active users and 5 radar targets. The performance of the ALS-based algorithm is better than that of the OMP algorithm, but as the SNR increases, its performance improvement becomes less significant compared to the OMP algorithm, indicating that the ALS-based algorithm has reached its performance limit. In contrast, since the OMP algorithm is sensitive to noise, its performance can be significantly improved by increasing the SNR. However, the ALS-based algorithm exhibits inferior performance compared to the proposed algorithm as it ignores the structure of the factor matrix, and the performance of the OMP algorithm is limited due to its sparsity assumption. In contrast, our proposed algorithm maintains better performance regardless of the numbers of active users and radar targets. For instance, the ADA performance can reach 0.98 at SNR = 20dB in the case of 10 active users and 5 radar targets and 0.99 at SNR = 10dB in the case of 5 active users and 10 radar targets, which verifies the effectiveness of our proposed algorithm on AUD. Additionally, the number of active users has a more significant impact on the results compared to the number of radar targets. This is because each additional user introduces multiple path parameters, while each additional radar target introduces only one path parameter. To be noticed, the performance of different algorithms is limited when the numbers of active users and
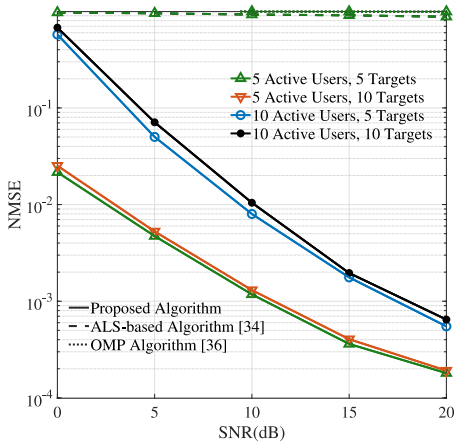
Fig. 4. Communication channel estimation performance of different algorithms under various SNRs.
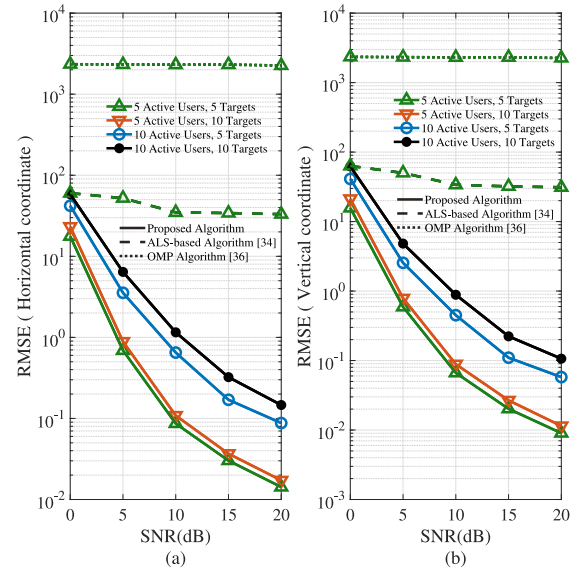

Fig. 5. Sensing position estimation performance of different algorithms under various SNRs.

Fig. 6. Channel estimation performance of proposed algorithm under various $\overline{K}$ at SNR = 15dB.

targets are 10 and 10, respectively, which is because the number of estimated path parameters increasing significantly.

In Fig. 4, the communication channel estimation performance is presented. It is shown that the communication channel estimation performance of the ALS-based algorithm and the OMP algorithm hardly improves with the increase of SNR, primarily due to the ALS algorithm neglecting the factor matrix structure and the OMP algorithm being constrained by its sparsity assumption. More specifically, when the SNR is 20dB, the NMSE can only be around 1, but the performance of ALS-based algorithm is still slightly better than that of the OMP algorithm. The main reason for the failure of these two algorithms is that the number of parameters required to be estimated exceeds the algorithm's capability. In contrast, in the case of 5 active users and 5 radar targets, our proposed algorithm can achieve an NMSE of nearly 10^{-4} when the SNR is 20dB due to the use of the Vandermonde characteristics of the factor matrix, which shows the superiority of our algorithm in communication parameter estimation.

Fig. 5 shows the sensing position estimation performance, with Fig. 5(a) and Fig. 5(b) illustrating the RMSE curves for estimated targets along the horizontal and vertical axes, respectively. Obviously, the performance of the ALS-based algorithm and the OMP algorithm have not improved significantly with the increase of SNR, while the performance of the proposed algorithm improves. Specifically, when SNR = 10dB, in the case of 5 active users and 5 radar targets, the RMSE performance of the ALS-based algorithm, which represents the positioning error, is approximately 30, while the RMSE performance of the OMP algorithm remains worse than the order 10^3. In contrast, under the same situation, the RMSE performance of our proposed algorithm on the horizontal and vertical axes can reach 10^{-1}, which proves the reliability of radar sensing resolution.

In Fig. 6, the channel estimation performance under various $\overline{K}$ at SNR = 15dB is shown. The NMSE for different combinations of active users and radar targets decreases as the number of training subcarriers $\overline{K}$ increases, due to the improved estimation accuracy of communication and radar path parameters. The curves for 5 active users with 5 or 10
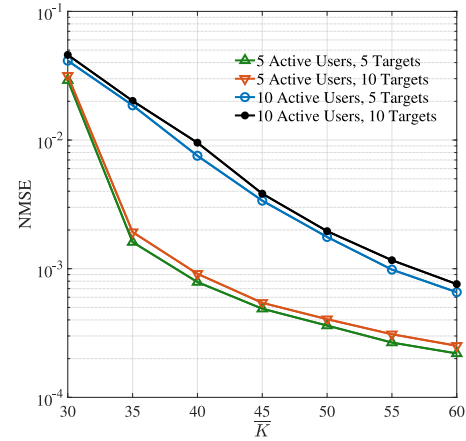
targets exhibit noticeable changes in slope, while those for 10 active users with 5 or 10 targets do not. This shows that when the number of path parameters to be estimated is small, the path parameter space of the system is relatively small. Consequently, before the training subcarrier resources reach saturation, the parameter estimation performance improves significantly. However, as the training subcarrier resources approach saturation, the system performance tends to be improved slightly, and further increase in $\overline{K}$ results in diminishing improvements, causing the noticeable changes in slope. For scenarios with more path parameters to estimate, such as 10 active users with 5 or 10 targets, more training resources are required, and the curves show gradual improvements without any noticeable change in slope.

Fig. 7 illustrates the channel estimation performance under various M_{BS} at SNR = 15dB. It can be seen that, as the number of the BS RF chains M_{BS} increases, the parameter estimation performance of the proposed algorithm under different numbers of active users and radars also improves. This
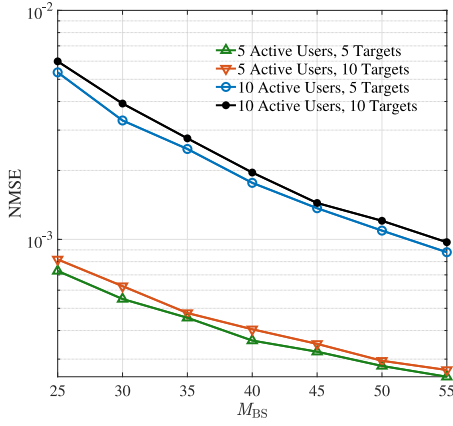
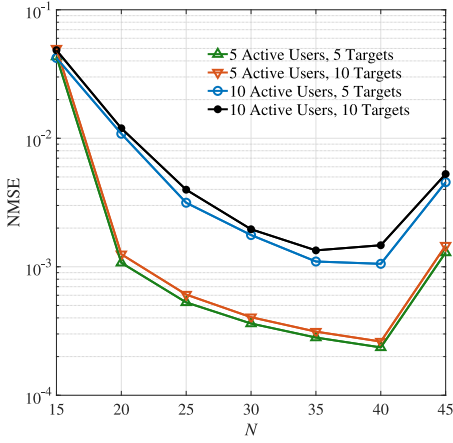Fig. 7. Channel estimation performance of proposed algorithm under various M_{BS} at SNR $= 15$dB.

Fig. 8. Channel estimation performance of proposed algorithm under various N at SNR $= 15$dB.

Fig. 9. Channel estimation performance of proposed algorithm under various N_{I} at SNR $= 15$dB.

is because the parameter estimation capability of the proposed algorithm can be improved by increasing the BS RF resources, and thus the estimation accuracy of the proposed algorithm also increases. When $M_{\mathrm{BS}} = 55$, the NMSE performance under different numbers of active users and radars can reach the order of 10^{-3}.

In Fig. 8, the channel estimation performance under various N at SNR $= 15$dB is presented. The curves of the different cases all show a same trend of first decreasing and then increasing as the number of frames N increases. For the case where the number of estimated parameters is small, the curve has an inflection point when $N = 20$, which cannot be observed when the number of estimated parameters is large. It is worth noting that when $N = 45$, the performance of the proposed algorithm decreases. This is because as the number of frames N increases, the Doppler shift accumulates excessively, thereby increasing the difficulty of parameter estimation and making the estimation performance worse.

Fig. 9 shows the channel estimation performance under various N_{I} at SNR $= 15$dB. The curves in this figure prove the convergence of the proposed JAI-PCE algorithm. It can be seen that the curves of the different cases tend to converge with the increase of the number of iterations N_{I}. Specifically,
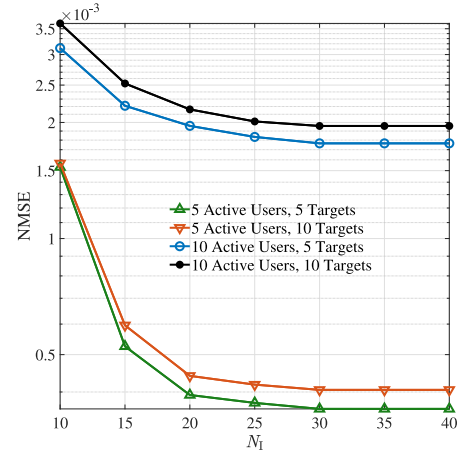
the number of iterations for the algorithm to converge in the different cases is about 30. The NMSE of 5 active users and 5 targets, 5 active users and 10 targets finally converges to about 4×10^{-4}, while the NMSE of 10 active users and 5 targets, and 10 active users and 10 targets finally converges to about 2×10^{-3}.

VI. CONCLUSION

In this paper, a scenario of joint AUD and ISAC was considered where an ISAC BS equipped with hybrid beamforming architectures concurrently serves large-scale communication users and performs target sensing. The channel and signal models of this scenario were first formulated, and transformed into a unified CPD-based form. Then, a matrix subspace-based method was proposed to accurately estimate the factor matrices where the communication and sensing parameters can be extracted. The complexity analysis of the proposed two-stage CPD-based unified communication channel and sensing target parameter estimation algorithm was further performed. To estimate the coupled parameters accurately, a JAI-PCE algorithm was developed, which mitigates the parameter identification issue associated with the CPD method by estimating the pilot sequence. Simulation results demonstrated that our proposed joint communication and sensing parameter estimation algorithm based on CPD exhibits exceptional performance in AUD, channel estimation, and radar sensing under large-scale user access, outperforming both the ALS-based algorithm and the OMP algorithm.

APPENDIX A
PROOF OF LEMMA 3

Proof: Considering the objective function of (44) in the $(i-1)$-th iteration, i.e., $g(\hat{\delta}_{l_a}^{(i-1)}, \hat{\nu}_{l_a}^{(i-1)}, \hat{\mathbf{F}}_{l_a}^{(i-1)}, \hat{\phi}_{l_a}^{(i-1)})$, we have

$$
g(\hat{\delta}_{l_a}^{(i-1)}, \hat{\nu}_{l_a}^{(i-1)}, \hat{\mathbf{F}}_{l_a}^{(i-1)}, \hat{\phi}_{l_a}^{(i-1)})
$$
$$
= \left\| \hat{\mathbf{a}}_{l_a}^{(2)} - \hat{\delta}_{l_a}^{(i-1)} \mathbf{\Gamma}\left(\hat{\nu}_{l_a}^{(i-1)}\right)\left(\hat{\mathbf{F}}_{l_a}^{(i-1)}\right)^T \mathbf{a}_{\mathrm{T}}\left(\hat{\phi}_{l_a}^{(i-1)}\right) \right\|_2^2 \quad (63)
$$

$$\overset{(a)}{\geq} g\left(\hat{\delta}_{l_a}^{(i)}, \hat{\nu}_{l_a}^{(i-1)}, \hat{\mathbf{F}}_{l_a}^{(i-1)}, \hat{\phi}_{l_a}^{(i-1)}\right) \tag{64}$$

$$\overset{(b)}{\geq} g\left(\hat{\delta}_{l_a}^{(i)}, \hat{\nu}_{l_a}^{(i)}, \hat{\mathbf{F}}_{l_a}^{(i-1)}, \hat{\phi}_{l_a}^{(i-1)}\right) \tag{65}$$

$$\overset{(c)}{\geq} g\left(\hat{\delta}_{l_a}^{(i)}, \hat{\nu}_{l_a}^{(i)}, \hat{\mathbf{F}}_{l_a}^{(i)}, \hat{\phi}_{l_a}^{(i-1)}\right) \tag{66}$$

$$\overset{(d)}{\geq} g\left(\hat{\delta}_{l_a}^{(i)}, \hat{\nu}_{l_a}^{(i)}, \hat{\mathbf{F}}_{l_a}^{(i)}, \hat{\phi}_{l_a}^{(i)}\right), \tag{67}$$

where (a), (b), (c), and (d) hold due to (46), (47), (48), and (49), respectively.

APPENDIX B
PROOF OF LEMMA 4

Proof: To simplify (46), let $n = 2$ in (41) and vectorize it, we have

$$\hat{\mathbf{a}}_{l_a}^{(2)} = \delta_{l_a} \mathbf{\Gamma}(\nu_{l_a}) \mathbf{F}_{l_a}^T \mathbf{a}_T(\phi_{l_a}) + \mathbf{e}_{l_a}, \tag{68}$$

where δ_{l_a}, ν_{l_a}, $\mathbf{F}_{l_a}$, and ϕ_{l_a} are the unknown parameters. According to the characteristic of the channels, we assume $\mathbf{e}_{l_a} \sim (\mathbf{0}, \sigma^2 \mathbf{I}_N)$, and the log-likelihood function of $\hat{\mathbf{a}}_{l_a}^{(2)}$ can be expressed as

$$L(\delta_{l_a}, \nu_{l_a}, \mathbf{F}_{l_a}, \phi_{l_a})$$
$$= -N \ln\left(\pi \sigma^2\right) - \frac{1}{\sigma^2} \left\| \hat{\mathbf{a}}_{l_a}^{(2)} - \delta_{l_a} \mathbf{\Gamma}(\nu_{l_a}) \mathbf{F}_{l_a}^T \mathbf{a}_T(\phi_{l_a}) \right\|_2^2$$
$$\propto -\left\| \hat{\mathbf{a}}_{l_a}^{(2)} - \delta_{l_a} \mathbf{\Gamma}(\nu_{l_a}) \mathbf{F}_{l_a}^T \mathbf{a}_T(\phi_{l_a}) \right\|_2^2. \tag{69}$$

The second derivative of this function with respect to δ_{l_a} is $2\|\mathbf{\Gamma}(\nu_{l_a})\mathbf{F}_{l_a}^T \mathbf{a}_T(\phi_{l_a})\|_2^2$, which is positive, thus the optimal δ_{l_a} can be obtained by setting $\frac{\partial L(\delta_{l_a}, \nu_{l_a}, \mathbf{F}_{l_a}, \phi_{l_a})}{\partial \delta_{l_a}} = 0$, and the equation of $\hat{\delta}_{l_a}^{(i)}$ can be given by

$$\hat{\delta}_{l_a}^{(i)} = \frac{\mathbf{a}_T^H\left(\hat{\phi}_{l_a}^{(i-1)}\right)\left(\hat{\mathbf{F}}_{l_a}^{(i-1)}\right)^* \mathbf{\Gamma}^{-1}\left(\hat{\nu}_{l_a}^{(i-1)}\right) \hat{\mathbf{a}}_{l_a}^{(2)}}{\left\| \left(\hat{\mathbf{F}}_{l_a}^{(i-1)}\right)^T \mathbf{a}_T\left(\hat{\phi}_{l_a}^{(i-1)}\right) \right\|_2^2}. \tag{70}$$

Considering the problem (47), the estimation of $\hat{\nu}_{l_a}^{(i)}$ can be obtained by

$$\hat{\nu}_{l_a}^{(i)} = \arg\min_{\nu_{l_a}} \left\| \hat{\mathbf{a}}_{l_a}^{(2)} - \hat{\delta}_{l_a}^{(i)} \mathbf{\Gamma}(\nu_{l_a}) \left(\hat{\mathbf{F}}_{l_a}^{(i-1)}\right)^T \mathbf{a}_T\left(\hat{\phi}_{l_a}^{(i-1)}\right) \right\|_2^2$$
$$= \arg\min_{\nu_{l_a}} \left\{ \left(\hat{\mathbf{a}}_{l_a}^{(2)}\right)^H \hat{\mathbf{a}}_{l_a}^{(2)} + |\hat{\delta}_{l_a}^{(i)}|^2 \mathbf{a}_T^H\left(\hat{\phi}_l^{(i-1)}\right)\left(\hat{\mathbf{F}}_{l_a}^{(i-1)}\right)^* \right.$$
$$\times \left(\hat{\mathbf{F}}_{l_a}^{(i-1)}\right)^T \mathbf{a}_T\left(\hat{\phi}_l^{(i-1)}\right) - \hat{\delta}_{l_a}^{(i)}\left(\hat{\mathbf{a}}_{l_a}^{(2)}\right)^H \mathbf{\Gamma}(\nu_{l_a})\left(\hat{\mathbf{F}}_{l_a}^{(i-1)}\right)^T$$
$$\times \mathbf{a}_T\left(\hat{\phi}_l^{(i-1)}\right) - \left(\hat{\delta}_{l_a}^{(i)}\left(\hat{\mathbf{a}}_{l_a}^{(2)}\right)^H \mathbf{\Gamma}(\nu_{l_a})\left(\hat{\mathbf{F}}_{l_a}^{(i-1)}\right)^T \right.$$
$$\left. \times \mathbf{a}_T\left(\hat{\phi}_l^{(i-1)}\right)\right)^H \right\}$$
$$= \arg\max_{\nu_{l_a}} \sum_{n=1}^N \mathrm{Re}\left(e^{j2\pi\nu_{l_a} n(K+N_{CP})T_s} \hat{\delta}_{l_a}^{(i)} \left[\hat{\mathbf{a}}_{l_a}^{(2)}\right]_{:,n}^* \right.$$
$$\left. \times \left(\hat{\mathbf{f}}_{l_a}^{(i-1)}(n)\right)^T \mathbf{a}_T\left(\hat{\phi}_l^{(i-1)}\right)\right). \tag{71}$$

According to (48), the estimation of $\hat{\mathbf{F}}_l^{(i)}$ can be obtained by

$$\hat{\mathbf{F}}_{l_a}^{(i)} = \arg\min_{\mathbf{F}_{l_a}} \left\| \left(\mathbf{\Gamma}(\hat{\nu}_{l_a}^{(i)})\right)^{-1} \hat{\mathbf{a}}_{l_a}^{(2)} - \hat{\delta}_{l_a}^{(i)} \mathbf{F}_{l_a}^T \mathbf{a}_T\left(\hat{\phi}_{l_a}^{(i-1)}\right) \right\|_2^2$$
$$= \arg\max_{\mathbf{F}_{l_a}} \left\| \frac{\mathbf{a}_T^H\left(\hat{\phi}_{l_a}^{(i-1)}\right) \mathbf{F}_{l_a}^* \mathbf{\Gamma}^{-1}\left(\hat{\nu}_{l_a}^{(i)}\right) \hat{\mathbf{a}}_{l_a}^{(2)}}{\mathbf{F}_{l_a}^T \mathbf{a}_T\left(\hat{\phi}_{l_a}^{(i-1)}\right)} \right\|_2^2$$
$$= \arg\max_{\mathbf{F}_{l_a}} \frac{\left| \mathbf{a}_T^H\left(\hat{\phi}_{l_a}^{(i-1)}\right) \mathbf{F}_{l_a}^* \mathbf{\Gamma}^{-1}\left(\hat{\nu}_{l_a}^{(i)}\right) \hat{\mathbf{a}}_{l_a}^{(2)} \right|^2}{\left\| \mathbf{F}_{l_a}^T \mathbf{a}_T\left(\hat{\phi}_{l_a}^{(i-1)}\right) \right\|_2^2}. \tag{72}$$

Finally, since (48) and (49) have similar structures, the estimation of $\hat{\phi}_{l_a}^{(i)}$ can be given by

$$\hat{\phi}_{l_a}^{(i)} = \arg\max_{\phi_{l_a}} \frac{\left| \mathbf{a}_T^H(\phi_{l_a})\left(\hat{\mathbf{F}}_{l_a}^{(i)}\right)^* \hat{\mathbf{\Gamma}}^{-1}\left(\hat{\nu}_{l_a}^{(i)}\right) \hat{\mathbf{a}}_{l_a}^{(2)} \right|^2}{\left\| \left(\hat{\mathbf{F}}_{l_a}^{(i)}\right)^T \mathbf{a}_T(\phi_{l_a}) \right\|_2^2}. \tag{73}$$

Therefore, the proof is completed.

REFERENCES

[1] B. Rong, "6G: The next horizon: From connected people and things to connected intelligence," *IEEE Wireless Commun.*, vol. 28, no. 5, pp. 8–8, Oct. 2021.

[2] A. Zhang, M. L. Rahman, X. Huang, Y. J. Guo, S. Chen, and R. W. Heath, "Perceptive mobile networks: Cellular networks with radio vision via joint communication and radar sensing," *IEEE Veh. Technol. Mag.*, vol. 16, no. 2, pp. 20–30, Jun. 2021.

[3] D. C. Nguyen et al., "6G Internet of Things: A comprehensive survey," *IEEE Internet Things J.*, vol. 9, no. 1, pp. 359–383, Jan. 2022.

[4] Y. Cui, F. Liu, X. Jing, and J. Mu, "Integrating sensing and communications for ubiquitous IoT: Applications, trends, and challenges," *IEEE Netw.*, vol. 35, no. 5, pp. 158–167, Sep./Oct. 2021.

[5] N. Wu et al., "AI-Enhanced integrated sensing and communications: Advancements, challenges, and prospects," *IEEE Commun. Mag.*, vol. 62, no. 9, pp. 144–150, Sep. 2024.

[6] L. Liu and W. Yu, "Massive connectivity with massive MIMO—Part I: Device activity detection and channel estimation," *IEEE Trans. Signal Process.*, vol. 66, no. 11, pp. 2933–2946, Jun. 2018.

[7] F. Liu et al., "Integrated sensing and communications: Toward dual-functional wireless networks for 6G and beyond," *IEEE J. Sel. Areas Commun.*, vol. 40, no. 6, pp. 1728–1767, Jun. 2022.

[8] R. Zhang et al., "Tensor decomposition-based channel estimation for hybrid mmWave massive MIMO in high-mobility scenarios," *IEEE Trans. Commun.*, vol. 70, no. 9, pp. 6325–6340, Sep. 2022.

[9] M. Ke, Z. Gao, Y. Wu, X. Gao, and R. Schober, "Compressive sensing-based adaptive active user detection and channel estimation: Massive access meets massive MIMO," *IEEE Trans. Signal Process.*, vol. 68, pp. 764–779, 2020.

[10] B. Wang, L. Dai, Y. Zhang, T. Mir, and J. Li, "Dynamic compressive sensing-based multi-user detection for uplink grant-free NOMA," *IEEE Commun. Lett.*, vol. 20, no. 11, pp. 2320–2323, Nov. 2016.

[11] Y. Du et al., "Efficient multi-user detection for uplink grant-free NOMA: Prior-information aided adaptive compressive sensing perspective," *IEEE J. Sel. Areas Commun.*, vol. 35, no. 12, pp. 2812–2828, Dec. 2017.

[12] L. Liu and W. Yu, "Massive connectivity with massive MIMO—Part II: Achievable rate characterization," *IEEE Trans. Signal Process.*, vol. 66, no. 11, pp. 2947–2959, Jun. 2018.

[13] J. Hu, I. Valiulahi, and C. Masouros, "ISAC receiver design: A learning-based two-stage joint data-and-target parameter estimation," *IEEE Wireless Commun. Lett.*, vol. 13, no. 8, pp. 2105–2109, Aug. 2024.

[14] M. F. Keskin, H. Wymeersch, and V. Koivunen, "MIMO-OFDM joint radar-communications: Is ICI friend or foe?" *IEEE J. Sel. Topics Signal Process.*, vol. 15, no. 6, pp. 1393–1408, Nov. 2021.

[15] X. Yang, H. Li, Q. Guo, J. A. Zhang, X. Huang, and Z. Cheng, "Sensing aided uplink transmission in OTFS ISAC with joint parameter association, channel estimation and signal detection," *IEEE Trans. Veh. Technol.*, vol. 73, no. 6, pp. 9109–9114, Jun. 2024.

[16] L. Lu, Z. Wang, Z. Gao, S. Chen, and H. V. Poor, "Block-sparse tensor recovery," *IEEE Trans. Inf. Theory*, vol. 70, no. 12, pp. 9293–9326, Dec. 2024.

[17] Z. Zhou, J. Fang, L. Yang, H. Li, Z. Chen, and R. S. Blum, "Low-rank tensor decomposition-aided channel estimation for millimeter wave MIMO-OFDM systems," *IEEE J. Sel. Areas Commun.*, vol. 35, no. 7, pp. 1524–1538, Jul. 2017.

[18] R. Zhang et al., "Integrated sensing and communication with massive MIMO: A unified tensor approach for channel and target parameter estimation," *IEEE Trans. Wireless Commun.*, vol. 23, no. 8, pp. 8571–8587, Aug. 2024.

[19] J. Wang, W. Zhang, Y. Chen, Z. Liu, J. Sun, and C.-X. Wang, "Time-varying channel estimation scheme for uplink MU-MIMO in 6G systems," *IEEE Trans. Veh. Technol.*, vol. 71, no. 11, pp. 11820–11831, Nov. 2022.

[20] T. Yang et al., "A unified tensor-based joint communication and sensing parameter estimation for ISAC with large-scale user access," in *Proc. Int. Conf. Signal Inf. Data Process. (ICSIDP)*, Nov. 2024, pp. 1–6.

[21] W. Chen, C. Liu, W. Wang, M. Peng, and W. Zhang, "Adaptive hybrid beamforming for UAV mmWave communications against asymmetric jitter," *IEEE Trans. Wireless Commun.*, vol. 23, no. 8, pp. 9432–9445, Aug. 2024.

[22] X. Hu, C. Liu, M. Peng, and Z. Zhong, "IRS-based integrated location sensing and communication for mmWave SIMO systems," *IEEE Trans. Wireless Commun.*, vol. 22, no. 6, pp. 4132–4145, Jun. 2023.

[23] M. Yuan et al., "Alternating optimization based hybrid transceiver designs for wideband millimeter-wave massive multiuser MIMO-OFDM systems," *IEEE Trans. Wireless Commun.*, vol. 22, no. 12, pp. 9201–9217, Dec. 2023.

[24] R. Ertel, P. Cardieri, K. Sowerby, T. Rappaport, and J. Reed, "Overview of spatial channel models for antenna array communication systems," *IEEE Pers. Commun.*, vol. 5, no. 1, pp. 10–22, Jan. 1998.

[25] J. A. Zhang, X. Huang, Y. J. Guo, J. Yuan, and R. W. Heath, "Multibeam for joint communication and radar sensing using steerable analog antenna arrays," *IEEE Trans. Veh. Technol.*, vol. 68, no. 1, pp. 671–685, Jan. 2019.

[26] G. Liu, A. Liu, R. Zhang, and M. Zhao, "Angular-domain selective channel tracking and Doppler compensation for high-mobility mmWave massive MIMO," *IEEE Trans. Wireless Commun.*, vol. 20, no. 5, pp. 2902–2916, May 2021.

[27] R. F. Tigrek, W. J. A. De Heij, and P. Van Genderen, "OFDM signals as the radar waveform to solve Doppler ambiguity," *IEEE Trans. Aerosp. Electron. Syst.*, vol. 48, no. 1, pp. 130–143, Jan. 2012.

[28] M. Heino et al., "Recent advances in antenna design and interference cancelation algorithms for in-band full duplex relays," *IEEE Commun. Mag.*, vol. 53, no. 5, pp. 91–101, May 2015.

[29] F. J. Soriano-Irigaray, J. S. Fernandez-Prat, F. J. Lopez-Martinez, E. Martos-Naya, O. Cobos-Morales, and J. T. Entrambasaguas, "Adaptive self-interference cancelation for full duplex radio: Analytical model and experimental validation," *IEEE Access*, vol. 6, pp. 65018–65026, 2018.

[30] L. Cheng, Y.-C. Wu, and H. V. Poor, "Probabilistic tensor canonical polyadic decomposition with orthogonal factors," *IEEE Trans. Signal Process.*, vol. 65, no. 3, pp. 663–676, Feb. 2017.

[31] A. Stegeman and N. D. Sidiropoulos, "On Kruskal's uniqueness condition for the Candecomp/Parafac decomposition," *Linear Algebra Appl.*, vol. 420, nos. 2–3, pp. 540–552, Jan. 2007.

[32] C. Qian, X. Fu, and N. D. Sidiropoulos, "Algebraic channel estimation algorithms for FDD massive MIMO systems," *IEEE J. Sel. Topics Signal Process.*, vol. 13, no. 5, pp. 961–973, Sep. 2019.

[33] M. Sørensen and L. De Lathauwer, "Blind signal separation via tensor decomposition with Vandermonde factor: Canonical polyadic decomposition," *IEEE Trans. Signal Process.*, vol. 61, no. 22, pp. 5507–5519, Nov. 2013.

[34] T. G. Kolda et al., "Tensor decompositions and applications," *SIAM Rev.*, vol. 51, no. 3, pp. 455–500, Sep. 2009.

[35] S. M. Kay, *Fundamentals of Statistical Signal Processing*. Upper Saddle River, NJ, USA: Prentice-Hall, 1993.

[36] J. A. Tropp and A. C. Gilbert, "Signal recovery from random measurements via orthogonal matching pursuit," *IEEE Trans. Inf. Theory*, vol. 53, no. 12, pp. 4655–4666, Dec. 2007.

Dongxuan He (Member, IEEE) received the B.S. degree in automation and the Ph.D. degree in information and communication systems from the Beijing Institute of Technology in 2013 and 2019, respectively, where he is currently an Assistant Professor with the School of Information and Electronics. From 2017 to 2018, he was a Visiting Student with the Singapore University of Technology and Design. From 2019 to 2022, he was a Postdoctoral Researcher with the Department of Electronic Engineering, Tsinghua University. His current interests include integrated sensing and communication, Terahertz communication, and AI empowered wireless communications. He was a recipient of the Best Paper Award from 2024 IEEE ICSIDP. He was also an Exemplary Reviewer of IEEE WIRELESS COMMUNICATIONS LETTERS. He is currently serving as a Guest Editor for IEEE OPEN JOURNAL OF THE COMMUNICATIONS SOCIETY, *Electronics*, and *Space: Science & Technology*.

Huazhou Hou (Member, IEEE) received the B.S. degree from the Beijing Institute of Technology in 2013, the M.S. and Ph.D. degrees from Northeast University in 2015 and 2020, respectively. From 2017 to 2019, he was a Joint Ph.D. Student with RMIT University, Melbourne, Australia. From 2020 to 2023, he was a Postdoctoral with Southeast University. He is currently an Associate Professor with the Pervasive Communication Research Center, Purple Mountain Laborites, Nanjing, China. His research interests include integrated sensing and communication, signal processing, and intelligent decision for unmanned systems. He has been awarded the 2024 IEEE ICSIDP Best Paper Award. He served as a Guest Editor for IEEE OPEN JOURNAL OF THE COMMUNICATIONS SOCIETY.

Hua Wang (Member, IEEE) received the Ph.D. degree from the Beijing Institute of Technology, Beijing, China, in 1999, where he is currently a Professor with the School of Information and Electronics. From February 2009 to January 2010, he was a Visiting Professor with the Department of Electrical Engineering, Arizona State University, Tempe, AZ, USA. His research interests include modulation and signal processing, wireless networking, and modem design and implementation for satellite communication.

Tiancheng Yang received the B.S. degree in electronic information engineering from Sichuan University, Sichuan, China, in 2018. He is currently pursuing the Ph.D. degree with the School of Information and Electronics, Beijing Institute of Technology, Beijing, China. His current research interests include interference management, deep reinforcement learning, tensor decomposition, and UAV communication. He was a recipient of the Best Paper Award from IEEE ICSIDP.

Hao Yin received the B.S. degree in microwave communication and the M.S. degree in communication and information systems from the Nanjing University of Posts and Telecommunications, Nanjing, China, in 1982 and 1987, respectively, and the Ph.D. degree in communication and information systems from the Beijing Institute of Technology, Beijing, China, in 1999. He is currently a Researcher with the Institute of Systems Engineering, Academy of Military Sciences, Beijing. His research interests include wireless communication networks and information systems. He is a Fellow of the Chinese Academy of Sciences and the China Institute of Communications.

Yongming Huang (Fellow, IEEE) received the B.S. and M.S. degrees from Nanjing University, Nanjing, China, in 2000 and 2003, respectively, and the Ph.D. degree in electrical engineering from Southeast University, Nanjing, in 2007. Since March 2007, he has been a Faculty with the School of Information Science and Engineering, Southeast University, where he is currently a Full Professor. He has also been the Director of the Pervasive Communication Research Center, Purple Mountain Laboratories, since 2019. From 2008 to 2009, he was visiting the Signal Processing Lab, Royal Institute of Technology, Stockholm, Sweden. He has published over 200 peer-reviewed papers, hold over 80 invention patents. His current research interests include intelligent 5G/6G mobile communications and millimeter wave wireless communications. He submitted around 20 technical contributions to IEEE standards, and was awarded a certificate of appreciation for outstanding contribution to the development of IEEE standard 802.11aj. He served as an Associate Editor for the IEEE TRANSACTIONS ON SIGNAL PROCESSING and a Guest Editor for IEEE JOURNAL ON SELECTED AREAS IN COMMUNICATIONS. He is currently an Editor-at-Large for IEEE OPEN JOURNAL OF THE COMMUNICATIONS SOCIETY.

Zhaocheng Wang (Fellow, IEEE) received the B.S., M.S., and Ph.D. degrees from Tsinghua University in 1991, 1993, and 1996, respectively. From 1996 to 1997, he was a Postdoctoral Fellow with Nanyang Technological University, Singapore. From 1997 to 1999, he was a Research Engineer/Senior Engineer with OKI Techno Centre Pvt. Ltd., Singapore. From 1999 to 2009, he was a Senior Engineer/Principal Engineer with Sony Deutschland GmbH, Germany. Since 2009, he has been a Professor with the Department of Electronic Engineering, Tsinghua University, where he is currently the Director of the Broadband Communication Key Laboratory, BNRist. His research interests include mmWave communications, optical wireless communications, and AI empowered wireless communications. He was a recipient of the 2016 IEEE Scott Helt Memorial Award, the 2016 IET Premium Award, the 2016 National Award for Science and Technology Progress (First Prize), the ICC2017 Best Paper Award, the 2018 IEEE ComSoc Asia–Pacific Outstanding Paper Award, and the 2020 IEEE ComSoc Leonard G. Abraham Prize.

Tony Q. S. Quek (Fellow, IEEE) received the B.E. and M.E. degrees in electrical and electronics engineering from the Tokyo Institute of Technology in 1998 and 2000, respectively, and the Ph.D. degree in electrical engineering and computer science from the Massachusetts Institute of Technology in 2008.

He is currently the Cheng Tsang Man Chair Professor with the Singapore University of Technology and Design (SUTD) and ST Engineering Distinguished Professor. He also serves as the Director of the Future Communications R&D Programme, the Head of ISTD Pillar, and the AI-on-RAN Working Group Chair in AI-RAN Alliance. His current research topics include wireless communications and networking, network intelligence, non-terrestrial networks, open radio access network, and 6G. He was honored with the 2008 Philip Yeo Prize for Outstanding Achievement in Research, the 2012 IEEE William R. Bennett Prize, the 2015 SUTD Outstanding Education Awards – Excellence in Research, the 2016 IEEE Signal Processing Society Young Author Best Paper Award, the 2017 CTTC Early Achievement Award, the 2017 IEEE ComSoc AP Outstanding Paper Award, the 2020 IEEE Communications Society Young Author Best Paper Award, the 2020 IEEE Stephen O. Rice Prize, the 2020 Nokia Visiting Professor, the 2022 IEEE Signal Processing Society Best Paper Award, and the 2024 IIT Bombay International Award For Excellence in Research in Engineering and Technology. He is a WWRF Fellow, and a Fellow of the Academy of Engineering Singapore.